Chemical Sample Processing for Combined Selenium Isotope and Selenium–tellurium Elemental Investigation of the Earth's Igneous Reservoirs

Aierken Yierpan[1], Stephan König[1], Jabrane Labidi[1], Timon Kurzawa[1], Michael G. Babechuk[2] and Ronny Schoenberg[1]

[1]Isotope Geochemistry, Department of Geosciences, University of Tübingen, Tübingen, Germany

[2]Department of Earth Sciences, Memorial University of Newfoundland, St. John's, Canada

Corresponding author: Aierken Yierpan (aierken.yierpan@uni-tuebingen.de)

Key point

- High-precision Se stable isotope and Se–Te concentration analyses from the same sample digest
- New Se isotope data for five international silicate reference materials and Se isotopic difference between basalts and chondrites
- Potential to study the Earth's igneous reservoirs and mantle perspective on the volatile evolution

Abstract

The redox-sensitive, chalcophile and volatile Se stable isotope system offers new perspectives to investigate the origin and evolution of terrestrial volatiles and the roles of magmatic and recycling processes in the development of the redox contrast between Earth's reservoirs. Selenium isotope systematics become more robust in a well-constrained petrogenetic context as can be inferred from Se–Te elemental signatures of sulfides and igneous rocks. In this study, we present a high-yield chemical sample processing method that allows the determination of Se–Te concentrations and Se isotope composition from the same sample digest of silicate rocks by hydride generation isotope dilution (ID) quadrupole inductively-coupled plasma mass spectrometry (ICP-MS) and double spike (DS) multicollector (MC)-ICP-MS, respectively. Our procedure yields ~80% Se–Te recoveries with quantitative separation of relevant interfering elements such as Ge and HG-buffering metals. Replicate analyses of selected international reference materials yield uncertainties better than 0.11‰ (2 s.d.) on $\delta^{82/76}$Se and 3% (r.s.d.) on Se concentration for DS MC-ICP-MS determinations for as low as ~10 ng sample Se. The precision of Se–Te concentration measurements by ID ICP-MS is better than 3% and 5% (r.s.d.) for total amounts of ~0.5–1 ng Se and ~0.2–0.5 ng Te, respectively. The basaltic reference materials have variable Se–Te contents, but their $\delta^{82/76}$Se values are rather uniform (on average 0.23 ± 0.14‰; 2 s.d.) and different from the chondritic value. This altogether provides the methodology and potential to extend the limited dataset of coupled Se isotope and Se–Te elemental systematics of samples relevant to study the terrestrial igneous inventory.

1. Introduction

Selenium and tellurium are moderately volatile (Lodders, 2003) and chalcophile elements (Guo et al., 1999; Hattori et al., 2002). They are present in the mantle at 2–3 orders of magnitude higher concentrations than expected from metal–silicate partitioning experiments performed at low pressure (<20 GPa; Rose-Weston et al., 2009). The broadly chondritic S–Se–Te elemental ratios in fertile peridotites (Wang & Becker, 2013) have been attributed to late accretion (i.e. the late veneer; Kimura et al., 1974; Morgan, 1986; McDonough & Sun, 1995). However, the sub-chondritic δ^{34}S of the silicate Earth indicates that the mantle S budget probably records core formation with limited sulfide incorporation rather than a post-core formation accretionary S addition (Labidi et al., 2013, 2016; Labidi & Cartigny, 2016). Moreover, some authors argue that the observed Se–Te signature of fertile peridotites are not primitive features of the mantle because

peridotites are generally affected by secondary magmatic processes (Harvey et al., 2015; König et al., 2014, 2015a, 2015b; Luguet et al., 2015).

Systematics of Se isotopes may contribute to placing constraints on these possible scenarios. If the Se budget was dominated by late-accreted materials and if no subsequent Se isotope fractionation of the upper mantle occurred, a chondritic Se isotope composition (Labidi et al., 2018; Vollstaedt et al., 2016) would be expected for the upper mantle. However, the scarcity of data sets regarding Se isotopes in mantle-derived rocks limits reasonable conclusions regarding either process. In order to evaluate the origin of Se isotope signatures in igneous rocks, the Se–Te elemental systematics are very useful. This is because of the chalcophile behaviours of both Se and Te with complementary partitioning into residual monosulfide solid solution vs metasomatic sulfide liquid, respectively (Brenan, 2015; König et al., 2014). Using Se–Te elemental systematics thus helps interpret isotopic signatures of Se in a constrained petrogenetic context, including partial melting, magmatic differentiation and metasomatic addition of base metal sulfides (e.g., Harvey et al., 2015; Jenner et al., 2015; König et al., 2014; Lissner et al., 2014; Luguet et al., 2015). Therefore, a combination of the Se–Te abundances and Se isotope analysis of igneous rocks may be useful for investigating the intrinsic origin and budget of these elements in the silicate Earth and during evolution of its reservoirs. Yet, to date, no such combined studies exist.

Following pioneering studies (Hertogen et al., 1980; Lorand & Alard, 2010; Morgan, 1986;), analytical advancements for combined Se–Te elemental analyses of silicate rocks have been made by hydride generation (HG) isotope dilution (ID) inductively-coupled plasma mass spectrometry (ICP-MS) measurements coupled with chemical purification such as thiol cotton fiber/powder (TCF/TCP) chemistry (König et al., 2012) and ion exchange chromatography (Wang et al., 2013). Different sample digestion techniques have been used: (1) inverse *aqua regia* digestion in a high-pressure asher (HPA-S) for peridotites (König et al., 2012; Wang & Becker, 2013, 2014; Wang et al., 2013), pyroxenites (Wang & Becker, 2015) and basalts (Wang et al., 2013); (2) hotplate HF digestion in perfluoroalkoxy alkane (PFA) beakers for peridotites (König et al., 2012, 2014, 2015a; Luguet et al., 2015) and basalts (Forrest et al., 2009; König et al., 2014; Lissner et al., 2014); (3) HF digestion in HPA-S or pressure bombs for a wide range of matrices, including peridotites, basalts and Martian meteorites (Wang et al., 2015; Wang & Becker, 2017); (4) inverse *aqua regia* (HPA-S) digestion followed by a hotplate HF-desilicification for peridotites (Harvey et al., 2015; König et al., 2012). While there are several rather comprehensive studies

regarding different chemical sample processing and associated limitations for analyses of highly siderophile element (HSE) abundances in mafic and ultramafic rocks (e.g., Dale et al., 2012; Day et. al., 2016; Ishikawa et al., 2014; Li et al., 2015; Meisel et al., 2003), few studies conducted comparative sample digestion experiments for Se–Te analyses (König et al., 2012, Wang & Becker, 2014; Wang et al., 2015).

Due to significant isotopic fractionation during Se oxyanion reduction (Krouse & Thode, 1962; Rees & Thode, 1966), Se isotope measurements have received increasing interest in biogeochemistry (Clark & Johnson, 2010; Ellis et al., 2003; Herbel et al., 2000, 2002; Johnson et al., 1999; Schilling et al., 2011a) and paleoenvironmental studies (Kipp et al., 2017; Layton-Matthews et al., 2013; Mitchell et al., 2012, 2016; Pogge Von Strandmann et al., 2015; Rouxel et al., 2004; Stüeken et al., 2015a, b; Zhu et al., 2014). Following important analytical advancements (Elwaer & Hintelmann, 2008; Layton-Matthews et al., 2006; Pogge von Strandmann et al., 2014; Rouxel et al., 2002; Stüeken et al., 2013; Zhu et al., 2008), Kurzawa et al. (2017) provided a precise and accurate measuring method for $\delta^{82/76}$Se with a consumption of as low as 5 ng Se, which allows the Se isotope determination of geological samples with low ng g^{-1} Se levels. To do so, it is necessary to establish a matrix-matched sample digestion and purification method that necessarily includes (1) complete Se extraction, (2) high chemistry recovery and (3) quantitative separation of HG-buffering transition metals and Ge that potentially causes significant isobaric interferences on ^{74}Se (e.g., Pogge von Strandmann et al., 2014; Stüeken et al., 2013).

In this study, we aim to combine the instrumental protocol for Se isotope analysis described by Kurzawa et al. (2017) with Se–Te concentration determinations by ID ICP-MS from a single digest of igneous rocks. We report on a series of comparative experiments on the international basaltic reference material BHVO-2 and discuss some of the major issues regarding sample digestion, such as sample heterogeneity, Se–Te extraction efficiency, sample-spike equilibration and Se–Te volatility. We present a suitable sample digestion and refined chemical purification method with high Se–Te recoveries, which enables precise and accurate Se isotope and Se–Te elemental analyses from the same rock digest using small amounts of sample materials. Our ultimate goal is to extend the limited data set of Se isotope composition and Se–Te concentrations of mantle-derived rocks in order to place firm constraints on the behavior of these elements in magmatic processes and their message regarding the origin and evolution of Earth's volatiles.

2. Reagents, samples and method

2.1. Reagents

Hydrochloric, hydrofluoric and nitric acids (Emsure®, Merck) used in this study were distilled using Savillex DST-1000 sub-boiling Teflon stills. All diluted acids were prepared with 18.2 MΩ·cm water and titrated on a molarity basis. All PFA vials were fluxed successively in reagent grade 3 M HCl, 5 M HNO_3 and 18.2 MΩ·cm H_2O at 120 °C for more than 48 h prior to use. The reducing solution for HG (0.1 M $NaBH_4$ in 0.07 M NaOH) was prepared fresh before each analytical session by dissolving sodium borohydride (analytical grade, Merck) and sodium hydroxide monohydrate (Suprapur®, Merck) in 18.2 MΩ·cm H_2O. Selenium standard solutions of NIST SRM 3149 and MH 495 (in 2 M HCl) were used for MC-ICP-MS analysis with concentrations of 15 or 30 ng mL^{-1}. The standard solutions used for ID ICP-MS measurements were diluted from NIST SRM 3149 and NIST SRM 3156 stock solutions to 0.5 ng mL^{-1}. A calibrated Se double spike (~52% ^{74}Se and ~47% ^{77}Se in 0.1 M HNO_3; Kurzawa et al., 2017) and Te single spike (~92% ^{125}Te in 1 M HNO_3; König et al., 2012) were used for our analyses.

2.2. Samples

Given the few studies regarding Se isotopes in mantle geochemistry, limited data of igneous reference materials measured by several working groups are available so far. In this study, we mainly used the international reference material BHVO-2 (Hawaiian basalt; splits #2375, #2481 and #3323) from the United States Geological Survey (USGS) for our sample digestion and chemical purification experiments because relatively consistent isotope dilution Se–Te concentration data are recently published for this material by different laboratories (König et al., 2012; Wang et al., 2015). The newly established sample processing scheme was then applied to other reference materials such as BCR-2 (Columbia River flood basalt, USGS), BE-N (continental intraplate basalt, Service d'Analyse des Roches et des Minéraux, France), BIR-1a (Icelandic basalt, USGS) and W-2a (diabase, USGS) to allow inter-laboratory comparison of future studies on a larger number of natural samples.

All reference materials used were supplied as finely ground powders. The BHVO-2 standard has a fairly wide range of particle sizes (supporting information Figure S1). To compare the Se–Te extraction efficiency of the HPA-S digestion between sample powders with different particle sizes, we reground two independent BHVO-2 splits (~6 g each) using a micro mill (Fritsch

Pulverisette 7 classic line). Particle size distribution of the reground material was determined using a laser particle sizer (Analysette 22 NanoTec) in the Application Laboratory of Fritsch, Germany. König et al. (2015a) demonstrated large whole-rock Se–Te concentration heterogeneities in peridotites. This was investigated for basalts in this study by analysis of BHVO-2 sieved fractions of <25 μm and >25 μm. Both fractions were further reground to preclude any potential sampling and digestion bias. All reground powders have particles ≤5 μm (supporting information Figure S1).

2.3. Sample Digestion

The extraction efficiency of the HPA-S technique for coupled Se isotope and Se–Te concentration analyses from the same sample digest was assessed using BHVO-2 under varying conditions, including sample size, acid volume, digestion temperature (supporting information Table S1) and particle size (supporting information Figure S1). A conventional hotplate HF digestion (König et al., 2012) was performed in parallel for comparison. We additionally carried out a series of extensive HF digestion experiments on BHVO-2 and BCR-2 following different protocols to evaluate some of the most common digestion related issues such as sample heterogeneity, sample-spike equilibration, effect of insoluble fluoride complexes and Se–Te volatility, with the aim to identify the most suitable digestion method for our routine analyses.

2.3.1. HPA-S (inverse *aqua regia*) digestion

The HPA-S (Anton Paar™, Graz) digestion was performed following the basic procedure outlined by Kurzawa et al. (2017). Briefly, about 0.2–1.1 g of BHVO-2 powder (n = 31) together with Se DS or Te single spike solutions were weighed into quartz glass vials and mixed with 2.5–10 mL inverse *aqua regia* (14.5 M HNO_3 and 10.5 M HCl, molar ratio 3:1). The digestion was carried out at 100 bar and different temperatures (220, 280, 320 °C) with a constant duration of 16 h. After the digestion, the supernatant was processed for Se–Te purification based on the protocol of Wang et al. (2013). The solid residue (n = 7) was analyzed for its Se content in order to assess Se extraction efficiency from the rock powder and potential Se degassing during ashing. To do so, the residue was first fluxed multiple (1–3) times with 18.2 MΩ·cm water in an ultrasonic bath for 30 min. After centrifugation for 15 min, the supernatant water was discarded and the residue was then transferred to a PFA beaker and dried down at 65 °C. The dry residue was carefully weighed with Se DS and processed following the HF digestion protocols described below.

2.3.2. Hotplate HF digestion

Sample powders ranging in weight from 0.05–1.2 g were mixed with Se and Te spike solutions and digested using a HF–HNO_3 mixture (1:5 volume ratio) in PFA beakers on a hotplate at 120 °C or 85 °C for 24 h. Solutions were subsequently evaporated at 65 °C. After this point, BHVO-2 and BCR-2 samples that were digested at 120 °C (n = 50 and 11, respectively) were processed following the protocol used by König et al. (2012) before the chemical purification. Briefly, the dry dissolved samples were taken up in 6 M HCl, heated at 100–130 °C for > 24 h, dried down at 65 °C and re-dissolved in 6 M HCl. The fluoride precipitates were removed via centrifugation and the supernatant solution was used for the subsequent TCF/TCP chemistry or chromatography. In order to examine the effect of insoluble fluorides for Se–Te analysis, additional HCl, HNO_3 and $HClO_4$ treatments were performed for several BHVO-2 (n = 4) in high-pressure PTFE vials with pressure bombs in an oven at 190 °C for 48 h to fully dissolve fluoride complexes (Cotta & Enzweiler, 2012; Langmyhr, 1967; Yokoyama et al., 1999). All HCl and HNO_3 solutions were evaporated to complete dryness at 65 °C. The $HClO_4$ solution was evaporated at 130 °C until ~10% solution remained in order to avoid potential Se loss (Stüeken et al., 2013) and directly taken up in 4 M HCl before chromatographic purification.

For all other samples that were digested at 85 °C, a modified protocol (i.e., our routine procedure) was used in combination with our ion exchange chromatography. The dry sample residues were dissolved and heated in 8 mL 6 M HCl at 130 °C on a hotplate for a minimum of 48 h, during which they were treated twice in an ultrasonic bath for 30 min. No visible fluoride precipitates were inspected at this point (for up to 0.55 g sample). Samples were subsequently evaporated to dryness at 85 °C, followed by two successive dissolutions and complete evaporations with 1 mL 10.5 M HCl. Finally, samples were taken up in 5 mL 4 M HCl and centrifuged for 10 min to separate transparent silica gels (e.g., Luais, 2012; Rouxel et al., 2006) prior to chromatographic purification.

In order to quantify and compare potential loss of Se–Te during the evaporation of HCl solutions, 7 BHVO-2 samples were digested and spiked only after the evaporation of 8 mL 6 M HCl and 2 mL 10.5 M HCl solutions to complete dryness at 65 (n = 4) or 85 °C (n = 3).

2.4. Chemical purification of Se and Te

2.4.1. TCF and TCP chemistry

Several BHVO-2 (n = 26) and BCR-2 (n = 4) samples with weights 0.25–1 g were digested with HF–HNO_3 and used for Se separation via TCF or TCP chemistry. The TCF and TCP batches (n = 5 and 1, respectively) were prepared from commercially available medical-grade cotton fiber and powder with analytical-grade thioglycolic acid, acetic anhydride, acetic acid and sulfuric acid (Merck) based on the methods described by König et al. (2012). Selenium was purified through columns filled with 0.15–0.3 g TCF and TCP (depending on the sample size) following the procedure of Rouxel et al. (2002) and Vollstaedt et al. (2016), respectively. After the separation and evaporation at 65 °C, a dark residue was observed. It was repeatedly treated with ~200 µL of 14.5 M HNO_3 and 30% H_2O_2 to remove residual organic matter. This step was followed by dissolution of the Se fractions in 1 mL 2 M HCl and centrifugation for 15 min. The supernatant was passed through a pre-cleaned 0.45 µm syringe filter (Millex®, Merck) to further eliminate residual fine organic particles (Vollstaedt et al., 2016) and then measured for Se isotope composition.

2.4.2. Ion exchange chromatography

When comparing the Se–Te extraction efficiencies of the HPA-S (inverse *aqua regia*) and hotplate HF digestions, BHVO-2 samples were purified for Se and/or Te using the ion exchange chromatography developed by Wang et al. (2013). This method was recently demonstrated to be applicable to high-precision analysis of Se isotopes in shales and basalts after the HPA-S digestion (Kurzawa et al., 2017). In contrast to HPA-S (inverse *aqua regia*) digestion that produces a relatively simple matrix (only ~12 wt.% of the BHVO-2 powder was dissolved; n = 13; supporting information Table S1; also see Xu et al., 2012), HF digestion results in whole-rock dissolution, posing additional difficulties on the ion exchange chromatography in terms of Se–Te recovery and separation of interference elements.

We tested existing purification protocols (supporting information Table S2) and propose an improved method in combination with our established HF digestion procedure. The new method utilized polypropylene columns (0.9 cm diameter and 8 cm bed height; Triskem, France) filled with 7 mL resin bed volume of Eichrom AG1-X8 (100–200 mesh chloride form) and Eichrom AG 50W-X8 (100–200 mesh hydrogen form) anion and cation exchange resins, respectively. A fresh

resin bed, pre-cleaned following a general laboratory procedure (e.g., successive cleaning with H_2O, HNO_3 and HCl), was used for each separation procedure. The columns were calibrated with 7 mL resin for up to 0.45 g mafic matrix. A complete procedure and elution profiles of Se–Te from NIST SRM 3149 and 3156 as well as BHVO-2 for each individual fraction (2.5 mL) are shown in Figure 1 and supporting information Table S3.

In the first stage, the anion exchange resin was cleaned with 10 mL 18.2 MΩ·cm water and conditioned with 10 mL 4 M HCl. The sample solution (5 mL 4 M HCl) was then loaded onto the column, followed by an addition of 9 mL 4 M HCl. Tellurium and iron are strongly retained by the resin in ≥2 M HCl (Fehr et al., 2004; Fornadel et al., 2014; Loss et al., 1990; Yi et al., 1998), whereas selenium is not adsorbed at HCl molarities of 4–7 M (Schönbächler and Fehr, 2014; Wang & Becker, 2014; Wang et al., 2015). The Se fraction was collected in 14 mL 4 M HCl together with most matrix elements and subsequently evaporated at 85 °C to complete dryness. Rinsing the resin with 10 mL of 2 M HCl–5 M HF mixture eluted almost all Fe while assuring complete retention of Te, probably as chloro- and fluoro-complexes. The resin was further rinsed with 4 mL 0.4 M HCl to elute residual Fe before collecting Te with 14 mL 0.4 M HCl. Separation of Fe may also be achieved by elution with 5 M HF only (Faris, 1960; Fehr et al., 2004; Wang et al., 2013), but we found that in that case, large amounts of eluent (>25 mL of 0.4 M HCl or 1 M HNO_3) were necessary to quantitatively elute Te. Besides, weak HCl was preferred over HNO_3 for Te elution as the latter more readily destroys the persistent $FeCl_4^-$ complex in the resin (Schoenberg & von Blanckenburg, 2005), resulting in more Fe in the Te eluate. Finally, the Te fractions were dried down at 85 °C to incipient dryness and directly taken up in 1 mL 2 M HCl for concentration analysis.

Complete separation of Fe from Te eluate is crucial as Fe significantly inhibits H_2Te formation during the analysis, reducing signal intensity (Yu et al., 1983). This effect was quantified by analyses of Fe-doped (ICP Fe standard solution, 1000 μg mL^{-1}) NIST SRM 3156 solutions (0.5 ng mL^{-1}), with Fe/Te mass ratio ranging between ~10^3 and 10^6 (supporting information Table S4).

In the second stage, the dry Se fraction was dissolved in 5 mL 0.1 M HNO_3 and placed in an ultrasonic bath for 30 min. When observed, insoluble fluorides were separated via 10-min centrifugation. Selenium was then purified through the cation column following the procedure

established by Wang et al. (2015) with small modifications. Briefly, the resin was rinsed with water and conditioned with 0.1 M HNO_3. The sample solution was then loaded onto the column, and Se was collected with another 9 mL 0.1 M HNO_3. In these conditions, other species such as the HG-buffering transition metals Co^{2+}, Ni^{2+}, Cu^{2+} and Pb^{2+} (Vijan & Leung, 1980; Welz & Melcher, 1984; Yu et al., 1983) are quantitatively retained on the resin (Davies, 2012). The Se fractions were dried down at 85 °C, followed by another complete dry-down in 2 mL 10.5 M HCl to remove extant NO_3^-. Finally, they were taken up in 1 mL 2 M HCl, from which an aliquot (100 µL) was measured to verify that all Ge was removed (see Section 2.5.1). In case of remaining Ge, the dry-down step at 85 °C was repeated (1–2 times) until a final 1 mL 2 M HCl solution was ready for Se isotope analysis. Note that in dependence on PFA beaker size, hotplate heating increments and laminar flow cooling effects, the specific temperature settings required for adequate hotplate temperatures may slightly vary in different laboratories. At this stage, we emphasize that the optimum temperature window (between 85 and 90 °C) is crucial for eliminating Ge from the sample solution while minimizing Se loss (see Section 4.2).

2.5. Instrumental analysis

2.5.1. DS MC-ICP-MS analysis

Analysis of Se isotope composition was performed on a ThermoFisher Scientific NeptunePlus™ MC-ICP-MS coupled with a HGX-200 (Cetac) hydride generator at the laboratory of the Isotope Geochemistry Group, University of Tübingen, Germany. Measurements were run in low-resolution mode with a Ni-Jet sample cone and Ni skimmer H-cone. Typical operating parameters, analytical procedure, interference corrections and double-spike inversion protocols were previously described in detail by Kurzawa et al. (2017). For most analyses in this study, ~10–35 ng mL^{-1} sample Se was used, which generated ^{82}Se signal intensities of ~350–1150 mV using a 10^{11} Ω amplifier resistor with an uptake rate of 0.181 mL min^{-1} under typical running conditions. The background level (typically ~3 mV on ^{82}Se) was determined on pure 2 M HCl before each standard and sample solution for on-peak-zero corrections. Washout times were typically 5 min. Selenium isotope ratios are expressed in the δ-notation relative to NIST SRM 3149 as per mil (‰) deviation following:

$$\delta^{82/76}Se_{Sample} = \left(\frac{^{82/76}Se_{Sample}}{^{82/76}Se_{NIST\ SRM\ 3149}} \right) \times 1000$$

The $\delta^{82/76}$Se values of sample and inter-laboratory standard MH 495 are always corrected against the average $\delta^{82/76}$Se value of two bracketing (concentration-matched) NIST SRM 3149 standards with 15 and 30 ng mL^{-1} Se. Kurzawa et al. (2017) reported a long-term external reproducibility of 0.11‰ (2 s.d.) on $\delta^{82/76}$Se using 15 ng mL^{-1} NIST SRM 3149 standard solution. The MH 495 standard analyzed together with the samples in this study yields mean $\delta^{82/76}$Se values of −3.24 ± 0.10‰ (2 s.d., n = 46) and −3.26 ± 0.06‰ (2 s.d., n = 32) for 15 and 30 ng mL^{-1} solutions, respectively (supporting information Table S5). This is in accordance with the value of −3.27 ± 0.13‰ (2 s.d., n = 100; on 15 ng mL^{-1} solution) reported by Kurzawa et al. (2017) and is within the range of previously published values (Carignan & Wen, 2007; Vollstaedt et al., 2016; Zhu et al., 2008).

Germanium is the main isobaric interference from the sample matrix in Se isotope analysis, but it cannot be fully separated from Se by our chromatography with the range of eluent molarities tested (e.g., 4–7 M HCl and 0.06–0.2 M HNO_3; but see Schilling et al., 2011b, 2014). However, it is efficiently eliminated during the evaporation of all HCl solutions at 85 °C (see Section 4.2). As a result, we observed $^{72}Ge/^{82}Se$ signal ratios <0.0002 (i.e., Ge/Se <0.0001) from all sample solutions with digested sample sizes <0.45 g, allowing us to fully neglect a ^{74}Ge interference correction. Note that the occurrence of As, Se and Br hydrides could also represent significant interferences (Pogge von Strandmann et al., 2014; Stüeken et al., 2013; Vollstaedt et al., 2016). However, all relevant hydride interferences are suppressed to undetectable levels by adding a controlled flux of methane in the plasma during the measurement (for details, see Floor et al., 2011; Kurzawa et al., 2017), and no further corrections were made after the on-peak-zero correction.

2.5.2. ID ICP-MS analysis

The Se and Te ID concentration measurements were carried out on a ThermoFisher Scientific iCAP-Qc quadrupole ICP-MS at the laboratory of the Isotope Geochemistry Group, University of Tübingen, Germany. For most analyses, aliquots of purified Se and Te fractions were prepared separately in 1 mL 2 M HCl to have 0.5–1.0 ng mL^{-1} Se and 0.15–0.5 ng mL^{-1} Te. Some sample unknowns were analyzed for Se concentrations directly after removing only Fe by the anion resin in order to swiftly obtain Se concentrations for adequate spiking for Se isotope analysis on new digests. The sample solutions were mixed with 2 M HCl and 0.1 M $NaBH_4$–0.07 M NaOH in a hydrideICP HG system (ESI) to reduce Se^{4+} and Te^{4+} oxyanions to their hydride forms, which

were transported by Ar (~1.08 L min^{-1}) to the plasma through a quartz cyclonic spray chamber. Measurements were performed in the iCAP-Qc STD mode to maximize signal sensitivity on the analyte isotopes, due to the reduction in sensitivity that can accompany the use of He kinetic energy discrimination (Chew et al., 2014). Each individual analysis consisted of 420 measurements of 3 points per peak of ^{77}Se and ^{78}Se for Se and ^{125}Te and ^{126}Te for Te with a dwell time of 0.03 s starting from the point of signal stabilization, which was usually achieved after ~1.2 min from the start of sample uptake. Every analytical session includes 4 standard solutions (0.5 ng mL^{-1} NIST SRM 3149 and 3156) measured before and after the sample unknowns. Under typical operating conditions with an uptake rate of ~0.41 mL/min, these standard solutions yield intensities of ~40,000 cps on ^{78}Se and ~55,000 cps on ^{126}Te, whereas the reagent blank (i.e., pure 2 M HCl) generally yields less than 13% and 3% of the respective signals. Unlike the HPA-S vial blanks that can sometimes be up to ~1 ng (Kurzawa et al., 2017), total procedural blanks (n = 10) from our established sample preparation procedures always yielded Se–Te signals that are indistinguishable from the background level on pure 2 M HCl. Taking the detection limit of the quadrupole ICP-MS as three times the standard deviation for each measured isotope in the reagent blank (Long & Winefordner, 1983), the maximum detection limits of the isotope dilution analysis calculated following the approach of Yu et al. (2002) are ~0.05 and ~0.007 ng mL^{-1} for Se and Te, respectively (for the comparison of ID detection limits on an Element XR sector field ICP-MS, see Wang & Becker, 2014).

A typical washout time of 2.5 min for solutions with Se concentrations of up to 5 ng mL^{-1} Se efficiently flushed the HG system. On the contrary, efficiency of Te washout was in some cases compromised by memory effects after ~10 samples. Elevated background levels may occur (up to 10 times the initial level), especially when Te fractions contain residual Fe after the purification. Note that our refined chromatographic protocol for Fe separation (by a HF–HCl mixture) efficiently addressed this issue (see Section 2.4.2). When still necessary in some cases, a prolonged >45 min washout was performed. Fehr et al. (2005) also reported long washout times of up to 60 min during Te isotope analysis using a desolvating nebulizer system. The primary source of the memory was identified as Te accumulation on the quartz injector and torch, which were cleaned with 0.1 M of HNO_3 or 0.5 M HCl for ~24 h after every 2 analytical sessions in order to ensure Te concentration data quality.

Selenium and tellurium concentrations of the samples were calculated using $^{77}Se/^{78}Se$ and $^{125}Te/^{126}Te$ ratios obtained after on-peak-zero and instrumental mass bias correction using the measured and natural ratios (Meija et al., 2016) of the NIST SRM 3149 and 3156 solutions. Although the Se and Te concentrations of these standards (both 0.5 ng mL^{-1}) in some cases do not overlap with the full range of sample concentrations (0.5–1.0 ng mL^{-1} Se and 0.15–0.5 ng mL^{-1} Te), we did not observe any associated uncertainty propagation on the corrected isotopic ratios, although the blank levels on each of the monitored masses are different. This might be due to the high washout efficiency for both Se and Te (with <10 samples in a session). The Se–Te analysis may in theory be affected by multiple isobaric and polyatomic interferences at monitored masses, but no further corrections were considered necessary. This is because any existing matrix-based oxides (e.g., $^{62}Ni^{16}O$, $^{109}Ag^{16}O$, $^{110}Pd^{16}O$ and $^{110}Cd^{16}O$) are prevented from entering the plasma by the hydride generator, whereas interferences from the carrier gas, analyte and cones (e.g., $^{40}Ar^{37}Cl$, $^{40}Ar^{38}Ar$, ^{78}Kr, $^{86}Kr^{40}Ar$, ^{126}Xe and $^{62}Ni^{16}O$) are considered to be constant over the course of a session and hence eliminated by the on-peak-zero correction. To evaluate the quantities of potential hydride interferences such as ^{76}GeH, ^{77}SeH, ^{124}SnH and ^{125}TeH, we monitored signal intensities at m/z 82, 83, 130 and 131 for ^{82}Se, ^{82}SeH, ^{130}Te and ^{130}TeH in 3 standard and BHVO-2 solutions containing 0.5–1.5 ng mL^{-1} Se and Te. The signals obtained at m/z 83 and 131 were identical to background levels within the Se and Te concentration range tested. Assuming $SeH^+/Se^+ = GeH^+/Ge^+$ and $TeH^+/Te^+ = SnH^+/Sn^+$, our results suggest that negligible interferences are generated from these hydrides.

The precision of the Se–Te concentration analyses is evaluated by replicate analyses of BHVO-2 with a wide range of sample sizes (~0.08–1.10 g) from different HF digestion batches (n = 61 and 24 for Se and Te, respectively) and chemical separation procedures (Figure 2 and supporting information Table S6). Despite these different methods applied, BHVO-2 yields consistent Se–Te concentrations with an average of 169 ± 3 ng g^{-1} Se (1 s.d., n = 61) and 14.2 ± 0.3 ng g^{-1} Te (1 s.d., n = 24; Figure 2). Based on these replicate analyses, the intermediate precision of our method for Se–Te concentration determination is estimated to be ~2% (expressed in r.s.d.). For comparison, some Se concentrations were determined on both quadrupole ICP-MS (by ID) and MC-ICP-MS (by DS inversion) using aliquots from the same sample digest and show excellent agreement (within ~3% variation) for all samples (supporting information Figure S2).

3. Results

3.1. Recoveries of Se and Te

Selenium and tellurium recoveries for BHVO-2 at different stages after digestion and chemical purification procedures are determined by the ID approach and/or comparing signal intensities against NIST SRM 3149 and 3156 standard solutions. Results are listed in supporting information Table S2. Selenium recoveries from the TCF and TCP chemistry are systematically low for BHVO-2 (<20%, n = 26) as well as BCR-2 (<15%, n = 4). Only Se concentrations were analyzed for these samples. Although this purification chemistry has the advantage of quantitatively separating Ge from Se (Rouxel et al., 2002), this technique was not pursued for subsequent Se isotope analysis due to the poor and variable Se recoveries obtained for basalts by several TCF and TCP batches (n = 5 and 1, respectively).

Selenium recoveries for BHVO-2 (digested with HF–HNO_3) from the new chromatographic purification procedure are 73–87% (n = 5) and 92–100% (n = 5) from the anion and cation exchange column, respectively, with a total procedural recovery of 70–83% (n = 16). The observed and expected signal intensities from samples relative to NIST SRM 3149 standard solutions show that the H_2Se formation efficiency exceeds 90% for all sample solutions after the 2-stage purification, indicating a near-quantitative removal of HG-buffering metals.

For Te in BHVO-2, we obtain 85–93% (n = 5) and 68–89% (n = 11) column chemistry and overall recovery, respectively. The lower overall recovery is mainly caused by the residual Fe that in some cases was not fully separated from Te, thereby inhibiting H_2Te formation. Analysis of Fe-doped standard solutions (see Section 2.4.2) shows that Te signals are highly sensitive to the amount of Fe: up to 40% signal loss can occur with Fe/Te = 5000 (Figure 3 and supporting information Table S4). Based on the difference between the (anion) column and overall recovery (i.e., ~15% signal suppression), an average Fe/Te ratio of ~1000–2000 is estimated for the BHVO-2 Te fraction. Low Te recoveries (10–30%) from peridotites observed by Wang et al. (2013) might also be due to the incomplete separation of Fe.

Overall, total procedural recoveries of Se and Te for all other samples (<0.45 g) are ~80% and ~75%, respectively. The Se and Te elution peaks can shift in the presence of matrix (see NIST SRM 3149 and 3156 versus BHVO-2 in Figure 1). However, in comparison to pure standard solution, the Se recoveries for BHVO-2 are only ~10% lower after anion and identical after cation

column chemistry. The Te column recovery is even identical between standard and matrix-bearing solutions (supporting information Table S3). This tentatively suggests that our chromatographic purification method is only slightly (if any) matrix-dependent.

As for the HCl evaporation experiments (see Section 2.3.2), we obtain 99–103% (n = 4) and 87–91% (n = 3) Se recoveries (determined by the ID method) from BHVO-2 when performing the evaporation at 65 and 85 °C, respectively. Two BHVO-2 samples spiked after the evaporation with ~10% Se loss at 85 °C yield higher $\delta^{82/76}$Se (0.42 ± 0.04‰; 2 s.d.) compared to our average value of BHVO-2 that are spiked prior to the digestion (Table 1). We obtain Te recoveries of ~100% at both evaporation temperatures for BHVO-2 (n = 5), as well as NIST SRM 3156 standard solutions (n = 5).

3.2. Se–Te concentrations

The BHVO-2 supplier and reground powders from the HPA-S digestions were analyzed for Se isotopes (hence also Se concentrations) or Te concentrations in order to evaluate Se and Te extraction efficiencies (supporting information Table S1). They yield average concentrations of 129 ± 8 ng g^{-1} Se (1 s.d., n = 25) and 12.5 ± 0.3 ng g^{-1} Te (1 s.d., n = 6). The reground powder alone yields 136 ± 5 ng g^{-1} Se (1 s.d., n = 6) and 12.7 ± 0.3 ng g^{-1} Te (1 s.d., n = 3), indistinguishable from the HPA-S total averages. These values display higher variations and are distinctly lower compared to the values from the HF-based digestions of BHVO-2 with average concentrations of 169 ± 3 ng g^{-1} Se (1 s.d., n = 61) and 14.2 ± 0.3 ng g^{-1} Te (1 s.d., n = 24; Figure 2). Note that the Se concentration of the solid residue after the HPA-S procedure is on average 37 ± 3 ng g^{-1} (1 s.d., n = 7; supporting information Table S1). When added to the HPA-S extracted fractions, this yields 173 ± 7 ng g^{-1} (1 s.d., n = 7), which matches the bulk BHVO-2 average (169 ± 3 ng g^{-1}; 1 s.d., n = 61) obtained from the HF digestion.

The Se–Te concentrations of reference materials obtained after the newly established sample digestion and purification protocols are listed in Table 1. Additional Se–Te concentration data for BHVO-2 and Se concentration data for BCR-2, BE-N, and W-2a from the HF-based digestion experiments using different purification protocols can be found in supporting information Table S6. The calculated uncertainties (r.s.d.) on all samples are better than ~3% and ~5% for Se and Te concentrations, respectively. Despite limited literature data, our BHVO-2 Se–Te concentrations overlap with the values of ~170 ng g^{-1} Se and ~11.9–14.4 ng g^{-1} Te reported by

König et al. (2012) and Wang et al. (2015). The reason why these two studies obtained similar Se (169 ± 3 ng g^{-1} and 170 ± 22 ng g^{-1}; 1 s.d.) but different Te concentrations (11.9 ± 0.7 ng g^{-1} and 14.4 ± 0.3 ng g^{-1}; 1 s.d.) for BHVO-2 remains unclear. We therefore compared our data with the combined range of these published data. Overall, our Se–Te concentrations of most samples are fairly comparable to the published data, but some significant differences are also observed (Table 1). For example, W-2a in this study yields Se concentration (107 ± 1 ng g^{-1}; 1 s.d., n = 8) that is significantly different from the published value of 5.2 ng g^{-1} (Forrest et al., 2009) but similar to the average value of 91 ± 13 ng g^{-1} (1 s.d.) from Savard et al. (2009). Also, BE-N Te concentration (1.02 ± 0.05 ng g^{-1}) is ~25–30% higher than those published by Lissner et al. (2014) and König et al. (2014). About ~7% relative difference is observed for BCR-2 Te data between this study and Lissner et al. (2014).

The BHVO-2 grain separates of >25 μm and <25 μm analyzed after the HF digestion yields distinct concentrations: 134 ± 2 and 200 ± 5 ng g^{-1} Se and 10.6 ± 0.4 and 18.9 ± 0.5 ng g^{-1} Te (all 1 s.d.; supporting information Table S7). Mass balance calculation of the bulk-rock Se–Te concentrations using weight fractions of these separates yields 167 ± 3 ng g^{-1} Se (1 s.d.) and 14.8 ± 0.3 ng g^{-1} Te (1 s.d.), in agreement with the average measured concentrations.

3.3. Se isotopic composition

The Se isotope compositions of BHVO-2 analyzed using the HPA-S and HF digestion techniques are listed in Table 1 and supporting information Table S1 and presented in Figure 4. Although the ID concentrations are significantly different as mentioned above, the $\delta^{82/76}$Se values for the bulk-rock BHVO-2 from the HF digestion and extracted fractions from the HPA-S digestion are indistinguishable: 0.18 ± 0.10‰ (2 s.d., n = 8) and 0.22 ± 0.10‰ (2 s.d., n = 12), respectively.

The bulk-rock Se isotope compositions of all international reference materials processed following the newly established sample processing scheme are listed in Table 1 and presented in Figure 5. Existing literature data for silicates, chondrites and troilites are also shown for comparison (Kurzawa et al., 2017; Labidi et al., 2018; Rouxel et al., 2002; Vollstaedt et al., 2016). The 2 s.d. uncertainties on $\delta^{82/76}$Se estimated over at least 5 different sample digestion batches are ≤0.11‰ for all samples. When the ^{82}Se signal is below 200 mV (~6.5 ng mL^{-1} Se), the internal precision (2 standard error, 2 s.e.) becomes higher than the analytical uncertainty. However, a

minimum of 6.5 ng Se still permits a high-precision Se isotope analysis (e.g., Kurzawa et al., 2017). In this study, more than 15 ng Se (up to 40 ng) was used for most analyses and the internal precision of a sample run is generally better than 0.06‰ (over 40 cycles). The $\delta^{82/76}$Se values of these reference materials range between −0.09 ± 0.11‰ (W-2a; 2 s.d., n = 6) and 0.29 ± 0.10‰ (BCR-2; 2 s.d., n = 5). The $\delta^{82/76}$Se value obtained for BE-N is 0.15 ± 0.10‰ (2 s.d., n = 5), similar within uncertainties to the previously published value of 0.37 ± 0.32‰ (relative to NIST SRM 3149; 2 s.d., n = 1; Rouxel et al., 2002; for the conversion, see Carignan & Wen, 2007). After HF digestion, BCR-2 yields comparable $\delta^{82/76}$Se within uncertainty to that obtained from HPA-S (inverse *aqua regia*) digestion (0.18 ± 0.03‰; 2 s.d., n = 3) by Kurzawa et al. (2017). The diabase W-2a yields distinctly lower $\delta^{82/76}$Se that does not overlap with any basaltic values.

4. Discussion

4.1. Comparison of the HPA-S (inverse *aqua regia*) and hotplate HF digestion

4.1.1. Se–Te extraction efficiency

Selenium and tellurium are chalcophile elements and considered to be primarily hosted by base metal sulfides and platinum group minerals in mantle rocks (Guo et al., 1999; Hattori et al., 2002; Lorand & Alard, 2010; König et al., 2015a). As these accessory phases are easily dissolved in inverse *aqua regia* at high temperature (e.g., Day et al., 2016; Li et al., 2015), a complete extraction of Se–Te from peridotites would be expected after HPA-S digestion. Despite heterogeneous distribution of sulfides in peridotites, several authors reported similar Se and/or Te abundances for peridotites using HPA-S or HF-based digestions (König et al., 2012, 2014, 2015a; Lissner et al., 2014; Wang et al., 2013, 2015; Wang & Becker, 2014). It is noteworthy that these groups analyzed UB-N (serpentinized lherzolite, SARM) as a reference material and obtained similar Se–Te abundances within uncertainties, regardless of whether silicate phases were dissolved by HF. This observation, together with the analytical results of a harzburgite sample (König et al., 2012), strongly argues for the quantitative control of the peridotite Se–Te budget by sulfides. In chondrites, Se also appears to be fully hosted by sulfides (Labidi et al., 2018; Vollstaedt et al., 2016; and references therein). The HPA-S (inverse *aqua regia*) digestion thus has been employed as an ideal digestion technique for combined determination of S–Se–Te and HSE abundances of mantle rocks, bulk chondrites and components of chondrites (Kadlag & Becker, 2015, 2016; Wang & Becker, 2013).

On the other hand, few comparative digestion experiments have been done on basalts. The basaltic reference material BHVO-1 (no longer commercially available from USGS) yields similar Se–Te ID concentrations from HPA-S (inverse *aqua regia*) and HF-based digestions (Makishima & Nakamura, 2009; Wang & Becker, 2014; Wang et al., 2015). Two previous studies (Kurzawa et al., 2017; Lissner et al., 2014) and this study obtain similar Se ID concentrations within uncertainty for another basaltic reference material BCR-2 (USGS) using these digestion techniques. However, basalts can have crystalline and glassy components. Selenium and tellurium, similar to sulfur, may be exsolved in sulfides and/or dissolved in the glassy matrices (e.g., Wykes et al., 2011, 2015). In this case, liberation of the dissolved Se–Te fractions requires HF-desilicification.

Relative to our BHVO-2 Se–Te concentrations obtained from HF digestion, the HPA-S digestion extracted 76 ± 5% and 88 ± 3% (1 s.d.) of the bulk-rock Se and Te, respectively (Figure 2). Note that the Se concentrations of the solid residue and extracted fractions of BHVO-2 after the HPA-S procedure sum up to the BHVO-2 bulk-rock average obtained after hotplate HF digestion (Section 3.2). The extraction efficiency of the HPA-S for Se seems independent from the sample size (~0.08–1.1 g), acid volume (2.5–10 mL) and ashing temperature (220–320 °C; see supporting information Table S1). Some sulfides can be enclosed in coarse silicate grains and remain shielded from acid digestion (Day et al., 2016). However, we observed nearly identical Se–Te extraction efficiency on both the supplier and reground powders (Figure 2 and supporting information Figure S1). This suggests that the population of exposed sulfides does not increase with decreasing particle sizes of the powder. Unless the sulfide grains are systematically smaller than silicate grains in the reground powder that ranges between 0.5 and 5 μm (Moore & Calk, 1971), our observation might suggest that most sulfides in BHVO-2 are quantitatively dissolved during the digestion. Similarly, all oxide phases are sufficiently dissolved in inverse *aqua regia* at high-temperature (Li et al., 2015). Therefore, we suggest that the unextracted portions of Se and Te from BHVO-2, which systematically represent ~25% and ~12% of the bulk-rock budget, are either dissolved in the glass matrix or hosted in the crystal lattice of silicate minerals (also see Chau & Riley, 1965; Hall & Pelchat, 1997a).

The results of this study support that the extraction of Se and Te from basalts using inverse *aqua regia* may depend on the sample matrix and partitioning of these elements between silicate phases (crystals and glass) and sulfides (e.g., Brenan, 2015; Kiseeva & Wood, 2017; Kiseeva et al., 2017), as previously suggested for some HSEs (e.g., Dale et al., 2012; Ishikawa et al., 2014;

Li et al., 2015). Therefore, the HPA-S (inverse *aqua regia*) digestion without HF-desilicification has to be used with caution for analyses of bulk-rock Se–Te concentrations and/or Se isotope composition of basalts and potentially other silicate melts.

4.1.2. Effect of insoluble fluorides during HF digestion

A typical disadvantage associated with HF-based digestion compared to the inverse *aqua regia* digestion is that many elements tend to coprecipitate with fluorides (e.g, Cotta & Enzweiler, 2012; Meisel et al., 2003; Takei et al., 2001; Yokoyama et al., 1999). Some authors speculated that Se and Te do not coprecipitate with fluorides but are dissolved in the supernatant HF solution as oxyanions (Makishima & Nakamura, 2009). Indeed, we did not observe any measurable Se or Te from fluoride precipitates (n = 5) that were separated and completely dissolved by multiple HCl treatments. Moreover, the low uncertainties and consistency of the BHVO-2 Se–Te ID concentrations obtained between different HF digestion procedures (see Section 2.3.2) seem to suggest a complete sample-spike equilibrium in the presence of fluoride precipitates, supporting that Se and Te do not coprecipitate with fluorides.

4.2. Volatile loss of Se–Te during the sample processing

Accurate determination of Se–Te and other volatile elements (such as S, Ge, As and Sb) in silicate rocks can be compromised by evaporative loss during solution treatment as hydride or halide species (Makishima et al., 2009). Formation of these species can be suppressed by the addition of strongly oxidizing HCl–HNO_3 or HBr–HNO_3 mixtures to the digestion acid (e.g., Hall & Pelchat, 1997a, b; Makishima & Nakamura, 2009). A combination of the inverse *aqua regia* digestion in HPA-S and the ID method may thus promote sample-spike equilibration and minimize analytical bias associated with the effects of Se–Te loss (König et al., 2012; Wang & Becker, 2014). In our experiment, the Se concentrations of the dissolved phases and residue of BHVO-2 from the HPA-S procedure sum up to 97 ± 6% (1 s.d., n = 7) of the bulk-rock Se concentration by ID. This suggests that Se degassing, if any, is efficiently prevented before equilibration of the dissolved sample fraction and spike.

Following HF digestion, Se and Te are probably present as aqueous oxyanions of Se^{4+} and/or Se^{6+} and Te^{4+} in the solution (Hall & Pelchat, 1997a; Kuldvere, 1989; Stüeken et al., 2013). During subsequent evaporation at 65 °C, these species may not be prone to degassing as volatile fluorides in the presence of rock matrix and HNO_3 (Marin et al., 2001; Makishima & Nakamura,

2009; but see Yi et al., 1998). Note that our HCl evaporation experiment conducted at 65 °C (after the evaporation of HF–HNO_3) yields full Se–Te recoveries from BHVO-2. This observation, together with the intermediate precision of our BHVO-2 Se–Te concentration data (r.s.d. = ~2%; Figure 2), suggests that both elements are not subject to evaporative losses following the HF digestion.

As for the subsequent HCl treatment for dissolving insoluble fluorides and converting total Se to Se^{4+} (Hill et al., 1995; Hall & Pelchat, 1997a), Se loss may indeed occur (Chau & Riley, 1965). This might be due to the formation of (1) volatile Se compounds such as hydride (H_2Se) and chlorides (Kurzawa et al., 2017; Schirmer et al., 2014; Vollstaedt et al., 2016) and/or (2) insoluble Se^0 (Langner, 2000; Marin et al., 2001; Tokunaga et al., 2013) that is unreactive with $NaBH_4$ during the analysis (Hall & Pelchat, 1997a). It has been suggested that evaporation of HCl solutions needs to be conducted below 80 °C to prevent Se loss (Layton-Matthews et al., 2006; Rouxel et al., 2002). However, despite the potential Se losses, we necessarily dried down all HCl solutions to complete dryness at 85 °C in order to quantitatively eliminate Ge as volatile $GeCl_4$ (boiling point 84 °C; see Lopez-Molinero et al., 2001; Luais, 2012; Makishima & Nakamura, 2009; Rouxel et al., 2006). Note that the double spike approach corrects for any isotopic fractionation associated with loss of Se as detailed by Kurzawa et al. (2017). We observed between negligible and up to 10% Se losses from BHVO-2 after multiple evaporations of HCl solutions at 65 and 85 °C, respectively (see Section 3.1). Kurzawa et al. (2017) reported large Se losses (up to 51%) from NIST SRM 3149 solution even at 65 °C. This indicates that the behavior of Se species in HCl in fact largely depends on the presence of sample matrix. On the other hand, we observed negligible evaporative Te losses from both standard (NIST SRM 3156) and BHVO-2 matrix solutions at 65 and 85 °C, reflecting different chemical behaviors of Se and Te in aqueous solutions (McPhail, 1995).

4.3. Sample heterogeneity

The reproducibility of HSE analysis is known to be compromised by sample heterogeneity (Meisel & Horan, 2016; and references therein). Similarly, based on the literature, Se–Te concentrations for a given sample can show large variabilities between replicate digestions (e.g., Forrest et al., 2009; König et al., 2012; Wang et al., 2015). This is more pronounced in peridotites even with a large sample size (up to 3 g; König et al., 2012). Furthermore, grain size experiments

on a harzburgite showed that coarse and fine fractions have quite different Se–Te concentrations and Se/Te ratios, emphasizing the importance of the mineralogy and sample size selection for precise Se–Te determinations in peridotites (König et al., 2015a).

The Se–Te concentrations of our BHVO-2 sieved fractions of >25 μm and <25 μm illustrate a similar sample heterogeneity in this basaltic reference material (supporting information Table S7). The Se/Te ratio of the fine fraction (10.6 ± 0.4) is lower than that of the coarse fraction (12.6 ± 0.5) and the bulk rock (11.9 ± 0.7; all 1 s.d.). For peridotites, the complementary Se/Te ratios in different grain separates are explained by the predominant stabilization of metasomatic Te-rich phases (e.g., tellurides) along interstitial grain boundaries after melt depletion (König et al., 2015a). In the case of basalt BHVO-2, it probably indicates predominant settling of tellurides or other high Te-bearing host phases (with lower Se/Te) along grain boundaries during cooling and crystallization of the melt.

Despite the heterogeneous distribution of Se–Te rich phases within the matrix, the variabilities of Se–Te concentrations obtained for bulk-rock BHVO-2 powders are always lower than ~3% (r.s.d.) at a range of sample sizes (~0.08–1.1 g; see supporting information Table S6 and Figure 2). Although the level of heterogeneity is predicted to be sample specific (Wang et al., 2015), low variabilities are also observed under intermediate precision conditions for the measured Se–Te concentrations (r.s.d. <5%) and $\delta^{82/76}$Se values (2 s.d. ≤0.11‰) in all reference materials with a wide range of Se–Te contents (~15–170 ng g^{-1} Se and ~1–14 ng g^{-1} Te). This suggests that the effect of sample heterogeneity might not be significant in Se–Te analysis of a melt-like matrix with digestion of down to 0.1 g sample powder.

4.4. The Se isotopic composition of igneous rocks

Identical $\delta^{82/76}$Se values after the HPA-S (inverse *aqua regia*) and hotplate HF digestions might indicate a Se isotopic homogeneity within a basaltic matrix (e.g., BHVO-2), despite seemingly different Se host phases as indicated by systematically lower and relatively variable Se concentrations obtained after the HPA-S digestion (Figure 4). However, for accurate analyses of combined Se isotope and Se concentration of bulk basalts, the use of HF is required to achieve complete Se extraction (see Section 4.1.1).

With the method presented, the $\delta^{82/76}$Se values of all analyzed reference materials are indistinguishable within 2 s.d. uncertainties from the previous estimate for the igneous silicate

Earth (0.33 ± 0.32‰; 2 s.d. analytical precision; Rouxel et al., 2002; Figure 5). Based on the basaltic reference materials and refined analytical precision (~0.11 ‰; 2 s.d.), we obtain an estimate of 0.23 ± 0.14‰ (2 s.d. of the mean). Interestingly, the basalts displaying this narrow range of $\delta^{82/76}$Se are from diverse geodynamic settings (e.g., ocean islands, plume-influenced mid-ocean ridges and continental settings). Despite markedly different Se–Te elemental systematics of these basalts (Table 1), their similar Se isotopic compositions overlapping with those of a peridotite (Rouxel et al., 2002) and basaltic glasses (from a lava lake near the Lucky Strike hydrothermal field; Rouxel et al., 2004) may either reflect their isotopically homogeneous source or secondary processes (e.g., Lissner et al., 2014; Jenner et al., 2015) that result in similar Se isotope and different Se–Te elemental signatures. On the same note, we point out that the resolvable differences of $\delta^{82/76}$Se values between these basalts and a diabase (W-2a) as well as a diorite (DR-N; Rouxel et al., 2002; Figure 5) require further investigation of different types of igneous rocks in order to assess if and how the respective emplacements or subtle petrogenetic differences have an effect on Se isotopes.

Despite some overlap within uncertainties, we note that the average $\delta^{82/76}$Se of basalts analyzed so far are higher than the average chondritic values of −0.30 ± 0.39‰ (2 s.d.; Vollstaedt et al., 2016) and −0.21 ± 0.31‰ (2 s.d.; Labidi et al., 2018). Perhaps more significantly, some basalts (BHVO-2 and BE-N) show $\delta^{82/76}$Se values similar to the estimate for carbonaceous chondrites (−0.01 ± 0.09‰; 2 s.d.), but all basalts show Se isotope signatures significantly different from those of ordinary and enstatite chondrites (−0.21 ± 0.10‰ and −0.40 ± 0.07‰, respectively; 2 s.d.; Labidi et al. 2018). However, a substantially extended data set on terrestrial melts and mantle rocks is still required to fully understand Se isotope variations in magmatic systems before constraining the isotopic composition of the bulk silicate Earth (BSE). This is a prerequisite for understanding the Se isotope and Se–Te elemental perspective on the origin and evolution of the Earth's volatiles.

5. Conclusion

This study presents a new and simplified chemical sample processing scheme that enables combined high-precision analyses of Se stable isotopes and Se–Te elemental abundances from the same rock digest of significantly small sample amounts using as low as ~6.5 ng Se by DS MC-ICP-MS (Kurzawa et al., 2017) and ~0.5 ng Se and ~0.15 ng Te by ID (quadrupole) ICP-MS. The

method includes a hotplate HF digestion and refined chromatographic purification that yields low blanks and high procedural recoveries of Se and Te (~80%). A complete separation of isobarically interfering Ge from Se is achieved via evaporation of HCl solutions at 85 °C. At the same time, previous equilibration of sample and ^{77}Se–^{74}Se double spike enables correction for any Se isotopic fractionation associated with minor Se losses. Low variability under intermediate precision conditions was obtained for each sample over at least 5 digestion batches, with calculated uncertainties better than ~0.11‰ (2 s.d.) on $\delta^{82/76}Se$ and 3% and 5% (r.s.d.) on Se and Te concentrations, respectively. The selected reference materials (BHVO-2, BIR-1a, BCR-2, BE-N and W-2a) are therefore considered to be rather homogeneous when digested strategically and recommended as Se isotope reference materials in future studies concerning igneous systems.

Although an identical $\delta^{82/76}Se$ value of BHVO-2 is observed using the HPA-S (inverse *aqua regia*) and HF digestion techniques, the former cannot fully extract Se and Te depending on the sample matrix and has to be used with caution in bulk-rock Se isotope and/or Se–Te abundance analyses of basaltic matrices. The presented sample preparation procedure in this study is optimized for basalts, but may be readily applied to other silicate matrices (e.g., ultramafic samples with resistant alloys) by employing HPA-S digestion followed by a hotplate HF-desilisification.

The basalts analyzed in this study have markedly distinct Se and Te contents, yet their Se isotopic compositions fall within the range of the igneous silicate Earth previously estimated by Rouxel et al. (2002) but exhibit a smaller variation with an average of 0.23 ± 0.14‰ (2 s.d.). Despite the demonstrated differences of $\delta^{82/76}Se$ between these basalts and main chondrite groups (Labidi et al., 2018; Vollstaedt et al., 2016), more systematic studies are required to investigate natural Se isotope variations in igneous systems in order to place firm constraints on the BSE and planetary-scale processes. At this point, the observed $\delta^{82/76}Se$ variations indicate the potential of Se isotopes as a future tracer for the origin and evolution of volatiles in the mantle.

Acknowledgement

This work was funded by an ERC Starting Grant (O_2RIGIN, 636808) to Stephan König. We thank Elmar Reitter, Martin Wille and Johannes Redlinger for their support during sample preparation and mass spectrometry analysis, and Markus Burnham for providing insight into hydride generation quadrupole ICP-MS analysis with his experience. We also thank Stephen A. Wilson (USGS) for providing the BHVO-2 particle size information and Fritsch (Germany) for

the particle size analysis. We greatly appreciate insightful reviews by Frances E. Jenner, Philip A.E. Pogge von Strandmann, Graeme M. Poole and an anonymous reviewer, as well as the editorial handling of Janne Blichert-Toft. All data used in this study are available in tables in the main text, Supporting Information and references.

References

Brenan, J. M. (2015). Se–Te fractionation by sulfide-silicate melt partitioning: Implications for the composition of mantle-derived magmas and their melting residues. *Earth and Planetary Science Letters*, *422*, 45-57. https://doi.org/10.1016/j.epsl.2015.04.011

Carignan, J. & Wen, H. J. (2007). Scaling NIST SRM 3149 for Se isotope analysis and isotopic variations of natural samples. *Chemical Geology*, *242*(3-4), 347-350. https://doi.org/10.1016/j.chemgeo.2007.03.020

Chau, Y. K. & Riley, J. P. (1965). The determination of selenium in sea water, silicates and marine organisms. *Analytica Chimica Acta*, *33*, 36-49. https://doi.org/10.1016/s0003-2670(01)84852-2

Chew, D. M., Donelick, R. A., Donelick, M. B., Kamber, B. S. & Stock, M. J. (2014). Apatite Chlorine Concentration Measurements by LA-ICP-MS. *Geostandards and Geoanalytical Research*, *38*(1), 23-35. https://doi.org/10.1111/j.1751-908X.2013.00246.x

Clark, S. K. & Johnson, T. M. (2010). Selenium Stable Isotope Investigation into Selenium Biogeochemical Cycling in a Lacustrine Environment: Sweitzer Lake, Colorado. *Journal of Environmental Quality*, *39*(6), 2200-2210. https://doi.org/10.2134/jeq2009.0380

Cotta, A. J. B. & Enzweiler, J. (2012). Classical and New Procedures of Whole Rock Dissolution for Trace Element Determination by ICP-MS. *Geostandards and Geoanalytical Research*, *36*(1), 27-50. https://doi.org/10.1111/j.1751-908X.2011.00115.x

Dale, C. W., Macpherson, C. G., Pearson, D. G., Hammond, S. J. & Arculus, R. J. (2012). Inter-element fractionation of highly siderophile elements in the Tonga Arc due to flux melting of a depleted source. *Geochimica et Cosmochimica Acta*, *89*, 202-225. https://doi.org/10.1016/j.gca.2012.03.025

Davies, C. M. (2012). Determination of distribution coefficients for cation exchange resin and optimisation of ion exchange chromatography for chromium separation for geological materials, (Master's thesis). UK: The University of Manchester.

Day, J. M. D., Waters, C. L., Schaefer, B. F., Walker, R. J. & Turner, S. (2016). Use of Hydrofluoric Acid Desilicification in the Determination of Highly Siderophile Element Abundances and Re–Pt–Os Isotope Systematics in Mafic-Ultramafic Rocks. *Geostandards and Geoanalytical Research*, *40*(1), 49-65. https://doi.org/10.1111/j.1751-908X.2015.00367.x

Ellis, A. S., Johnson, T. M., Herbel, M. J. & Bullen, T. D. (2003). Stable isotope fractionation of selenium by natural microbial consortia. *Chemical Geology*, *195*(1-4), 119-129. https://doi.org/10.1016/S0009-2541(02)00391-1

Elwaer, N. & Hintelmann, H. (2008). Selective separation of selenium (IV) by thiol cellulose powder and subsequent selenium isotope ratio determination using multicollector inductively

coupled plasma mass spectrometry. *Journal of Analytical Atomic Spectrometry*, *23*(5), 733-743. https://doi.org/10.1039/b801673a

Faris, J. P. (1960). Adsorption of Elements from Hydrofluoric Acid by Anion Exchange. *Analytical Chemistry*, *32*(4), 520-522. https://doi.org/10.1021/ac60160a019

Fehr, M. A., Rehkamper, M. & Halliday, A. N. (2004). Application of MC-ICPMS to the precise determination of tellurium isotope compositions in chondrites, iron meteorites and sulfides. *International Journal of Mass Spectrometry*, *232*(1), 83-94. https://doi.org/10.1016/j.ijms.2003.11.006

Fehr, M. A., Rehkämper, M., Halliday, A. N., Wiechert, U., Hattendorf, B., Günther, D., Ono, S., Eigenbrode, J. L. & Rumble, D. (2005). Tellurium isotopic composition of the early solar system—A search for effects resulting from stellar nucleosynthesis, ^{126}Sn decay, and mass-independent fractionation. *Geochimica et Cosmochimica Acta*, *69*(21), 5099-5112. https://doi.org/10.1016/j.gca.2005.04.020

Floor, G. H., Millot, R., Iglesias, M. & Negrel, P. (2011). Influence of methane addition on selenium isotope sensitivity and their spectral interferences. *Journal of Mass Spectrometry*, *46*(2), 182-188. https://doi.org/10.1002/jms.1880

Fornadel, A. P., Spry, P. G., Jackson, S. E., Mathur, R. D., Chapman, J. B. & Girard, I. (2014). Methods for the determination of stable Te isotopes of minerals in the system Au–Ag–Te by MC-ICP-MS. *Journal of Analytical Atomic Spectrometry*, *29*(4), 623-637. https://doi.org/10.1039/c3ja50237f

Forrest, A., Kingsley, R. & Schilling, J. G. (2009). Determination of Selenium and Tellurium in Basalt Rock Reference Materials by Isotope Dilution Hydride Generation-Inductively Coupled Plasma-Mass Spectrometry (ID-HG-ICP-MS). *Geostandards and Geoanalytical Research*, *33*(2), 261-269. https://doi.org/10.1111/j.1751-908X.2009.00841.x

Guo, J. F., Griffin, W. L. & O'Reilly, S. Y. (1999). Geochemistry and origin of sulphide minerals in mantle xenoliths: Qilin, southeastern China. *Journal of Petrology*, *40*(7), 1125-1149. https://doi.org/10.1093/petroj/40.7.1125

Hall, G. E. M. & Pelchat, J.-C. (1997a). Analysis of Geological Materials for Bismuth, Antimony, Selenium and Tellurium by Continuous Flow Hydride Generation Inductively Coupled Plasma Mass Spectrometry Part 2. Methodology and Results. *Journal of Analytical Atomic Spectrometry*, *12*(1), 103-106. https://doi.org/10.1039/a605399h

Hall, G. E. M. & Pelchat, J.-C. (1997b). Determination of As, Bi, Sb, Se and Te in Fifty Five Reference Materials by Hydride Generation ICP-MS. *Geostandards and Geoanalytical Research*, *21*(1), 85-91. https://doi.org/10.1111/j.1751-908X.1997.tb00534.x

Harvey, J., König, S. & Luguet, A. (2015). The effects of melt depletion and metasomatism on highly siderophile and strongly chalcophile elements: S–Se–Te–Re–PGE systematics of peridotite xenoliths from Kilbourne Hole, New Mexico. *Geochimica et Cosmochimica Acta*, *166*, 210-233. https://doi.org/10.1016/j.gca.2015.06.028

Hattori, K. H., Arai, S. & Clarke, D. B. (2002). Selenium, tellurium, arsenic and antimony contents of primary mantle sulfides. *Canadian Mineralogist*, *40*, 637-650. https://doi.org/10.2113/gscanmin.40.2.637

Herbel, M. J., Johnson, T. M., Oremland, R. S. & Bullen, T. D. (2000). Fractionation of selenium isotopes during bacterial respiratory reduction of selenium oxyanions. *Geochimica et Cosmochimica Acta*, *64*(21), 3701-3709. https://doi.org/10.1016/S0016-7037(00)00456-7

Herbel, M. J., Johnson, T. M., Tanji, K. K., Gao, S. & Bullen, T. D. (2002). Selenium stable isotope ratios in California agricultural drainage water management systems. *Journal of Environmental Quality*, *31*(4), 1146-1156. https://doi.org/10.2134/jeq2002.1146

Hertogen, J., Janssens, M. J. & Palme, H. (1980). Trace-Elements in Ocean Ridge Basalt Glasses: Implications for Fractionations during Mantle Evolution and Petrogenesis. *Geochimica et Cosmochimica Acta*, *44*(12), 2125-2143. https://doi.org/10.1016/0016-7037(80)90209-4

Hill, S. J., Pitts, L. & Worsfold, P. (1995). Investigation into the Kinetics of Selenium(VI) Reduction Using Hydride Generation Atomic Fluorescence Detection. *Journal of Analytical Atomic Spectrometry*, *10*(5), 409-411. https://doi.org/10.1039/ja9951000409

Ishikawa, A., Senda, R., Suzuki, K., Dale, C. W. & Meisel, T. (2014). Re-evaluating digestion methods for highly siderophile element and ^{187}Os isotope analysis: Evidence from geological reference materials. *Chemical Geology*, *384*, 27-46. https://doi.org/10.1016/j.chemgeo.2014.06.013

Jenner, F. E., Hauri, E. H., Bullock, E. S., König, S., Arculus, R. J., Mavrogenes, J. A., Mikkelson, N. & Goddard, C. (2015). The competing effects of sulfide saturation versus degassing on the behavior of the chalcophile elements during the differentiation of hydrous melts. *Geochemistry, Geophysics, Geosystems*, *16*(5), 1490-1507. https://doi.org/10.1002/2014gc005670

Johnson, T. M., Herbel, M. J., Bullen, T. D. & Zawislanski, P. T. (1999). Selenium isotope ratios as indicators of selenium sources and oxyanion reduction. *Geochimica et Cosmochimica Acta*, *63*(18), 2775-2783. https://doi.org/10.1016/S0016-7037(99)00279-3

Kadlag, Y. & Becker, H. (2015). Fractionation of highly siderophile and chalcogen elements in components of EH3 chondrites. *Geochimica et Cosmochimica Acta*, *161*, 166-187. https://doi.org/10.1016/j.gca.2015.04.022

Kadlag, Y. & Becker, H. (2016). ^{187}Re–^{187}Os systematics, highly siderophile element, S–Se–Te abundances in the components of unequilibrated L chondrites. *Geochimica et Cosmochimica Acta*, *172*, 225-246. https://doi.org/10.1016/j.gca.2015.09.026

Kimura, K., Lewis, R. S. & Anders, E. (1974). Distribution of gold and rhenium between nickel–iron and silicate melts: implications for the abundance of siderophile elements on the Earth and Moon. *Geochimica et Cosmochimica Acta*, *38*(5), 683-701. https://doi.org/10.1016/0016-7037(74)90144-6

Kipp, M. A., Stüeken, E. E., Bekker, A. & Buick, R. (2017). Selenium isotopes record extensive marine suboxia during the Great Oxidation Event. *Proceedings of the National Academy of Sciences of the United States of America*, *114*(5), 875-880. https://doi.org/10.1073/pnas.1615867114

Kiseeva, E. S. & Wood, B. J. (2017). *Partitioning of As, Se, Te and Bi between sulphide and silicate liquids.* Paper presented at Annual V.M. Goldschmidt Conference, Paris, France

Kiseeva, E. S., Fonseca, R. O. C. & Smythe, D. J. (2017). Chalcophile Elements and Sulfides in

the Upper Mantle. *Elements*, *13*(2), 111-116. https://doi.org/10.2113/gselements.13.2.111

König, S., Luguet, A., Lorand, J. P., Wombacher, F. & Lissner, M. (2012). Selenium and tellurium systematics of the Earth's mantle from high precision analyses of ultra-depleted orogenic peridotites. *Geochimica et Cosmochimica Acta*, *86*, 354-366. https://doi.org/10.1016/j.gca.2012.03.014

König, S., Lorand, J. P., Luguet, A. & Pearson, D. G. (2014). A non-primitive origin of near-chondritic S–Se–Te ratios in mantle peridotites; implications for the Earth's late accretionary history. *Earth and Planetary Science Letters*, *385*, 110-121. https://doi.org/10.1016/j.epsl.2013.10.036

König, S., Lissner, M., Lorand, J. P., Bragagni, A. & Luguet, A. (2015a). Mineralogical control of selenium, tellurium and highly siderophile elements in the Earth's mantle: Evidence from mineral separates of ultra-depleted mantle residues. *Chemical Geology*, *396*, 16-24. https://doi.org/10.1016/j.chemgeo.2014.12.015

König, S., Lissner, M., Lorand, J.-P., Bragagni, A. & Luguet, A. (2015b). Reply to the comment on "A non-primitive origin of near-chondritic S–Se–Te ratios in mantle peridotites: Implications for the Earth's late accretionary history" by König S. et al. [Earth Planet. Sci. Lett. 385 (2014) 110–121]. *Earth and Planetary Science Letters*, *417*, 167-169. https://doi.org/10.1016/j.epsl.2013.10.036

Krouse, H. R. & Thode, H. G. (1962). Thermodynamic Properties and Geochemistry of Isotopic Compounds of Selenium. *Canadian Journal of Chemistry*, *40*(2), 367-375. https://doi.org/10.1139/v62-055

Kuldvere, A. (1989). Extraction of Geological-Materials with Mineral Acids for the Determination of Arsenic, Antimony, Bismuth and Selenium by Hydride Generation Atomic-Absorption Spectrometry. *Analyst*, *114*(2), 125-131. https://doi.org/10.1039/an9891400125

Kurzawa, T., König, S., Labidi, J., Yierpan, A. & Schoenberg, R. (2017). A method for Se isotope analysis of low ng-level geological samples via double spike and hydride generation MC-ICP-MS. *Chemical Geology*, *466*, 219-228. https://doi.org/10.1016/j.chemgeo.2017.06.012

Labidi, J. & Cartigny, P. (2016). Negligible sulfur isotope fractionation during partial melting: Evidence from Garrett transform fault basalts, implications for the late-veneer and the hadean matte. *Earth and Planetary Science Letters*, *451*, 196-207. https://doi.org/10.1016/j.epsl.2016.07.012

Labidi, J., Cartigny, P. & Moreira, M. (2013). Non-chondritic sulphur isotope composition of the terrestrial mantle. *Nature*, *501*(7466), 208-211. https://doi.org/10.1038/nature12490

Labidi, J., Shahar, A., Le Losq, C., Hillgren, V. J., Mysen, B. O. & Farquhar, J. (2016). Experimentally determined sulfur isotope fractionation between metal and silicate and implications for planetary differentiation. *Geochimica et Cosmochimica Acta*, *175*, 181-194. https://doi.org/10.1016/j.gca.2015.12.001

Labidi, J., König, S., Kurzawa, T., Yierpan, A. & Schoenberg, R. (2018). The selenium isotopic variations in chondrites are mass-dependent; Implications for sulfide formation in the early solar system. *Earth and Planetary Science Letters*, *481*, 212-222. https://doi.org/10.1016/j.epsl.2017.10.032

Langmyhr, F. J. (1967). Removal of Hydrofluoric Acid by Evaporation in Presence of Sulfuric or Perchloric Acids. *Analytica Chimica Acta*, *39*(4), 516-&. https://doi.org/10.1016/S0003-2670(01)80548-1

Langner, B. E. (2000) Selenium and Selenium Compounds, *Ullmann's Encyclopedia of Industrial Chemistry*. https://doi.org/10.1002/14356007.a23_525

Layton-Matthews, D., Leybourne, M. I., Peter, J. M. & Scott, S. D. (2006). Determination of selenium isotopic ratios by continuous-hydride-generation dynamic-reaction-cell inductively coupled plasma-mass spectrometry. *Journal of Analytical Atomic Spectrometry*, *21*(1), 41-49. https://doi.org/10.1039/b501704a

Layton-Matthews, D., Leybourne, M. I., Peter, J. M., Scott, S. D., Cousens, B. & Eglington, B. M. (2013). Multiple sources of selenium in ancient seafloor hydrothermal systems: Compositional and Se, S, and Pb isotopic evidence from volcanic-hosted and volcanic-sediment-hosted massive sulfide deposits of the Finlayson Lake District, Yukon, Canada. *Geochimica et Cosmochimica Acta*, *117*, 313-331. https://doi.org/10.1016/j.gca.2013.05.002

Li, J., Zhao, P. P., Liu, J. G., Wang, X. C., Yang, A. Y., Wang, G. Q. & Xu, J. F. (2015). Reassessment of Hydrofluoric Acid Desilicification in the Carius Tube Digestion Technique for Re–Os Isotopic Determination in Geological Samples. *Geostandards and Geoanalytical Research*, *39*(1), 17-30. https://doi.org/10.1111/j.1751-908X.2014.00299.x

Lissner, M., König, S., Luguet, A., le Roux, P. J., Schuth, S., Heuser, A. & le Roex, A. P. (2014). Selenium and tellurium systematics in MORBs from the southern Mid-Atlantic Ridge (47–50 °S). *Geochimica et Cosmochimica Acta*, *144*, 379-402. https://doi.org/10.1016/j.gca.2014.08.023

Lodders, K. (2003). Solar system abundances and condensation temperatures of the elements. *Astrophysical Journal*, *591*(2), 1220-1247. https://doi.org/10.1086/375492

Long, G. L. & Winefordner, J. D. (1983). Limit of Detection A Closer Look at the IUPAC Definition. *Analytical Chemistry*, *55*(07), 712A-724A. https://doi.org/10.1021/ac00258a724

Lopez-Molinero, A., Villareal, A., Andia, D., Velilla, C. & Castillo, J. R. (2001). Volatile germanium tetrachloride for sample introduction and germanium determination by inductively coupled plasma atomic emission spectroscopy. *Journal of Analytical Atomic Spectrometry*, *16*(7), 744-749. https://doi.org/10.1039/b009937f

Lorand, J. P. & Alard, O. (2010). Determination of selenium and tellurium concentrations in Pyrenean peridotites (Ariege, France): New insight into S/Se/Te systematics of the upper in mantle samples. *Chemical Geology*, *278*(1-2), 120-130. https://doi.org/10.1016/j.chemgeo.2010.09.007

Loss, R. D., Rosman, K. J. R. & Delaeter, J. R. (1990). The Isotopic Composition of Zinc, Palladium, Silver, Cadmium, Tin, and Tellurium in Acid-Etched Residues of the Allende Meteorite. *Geochimica et Cosmochimica Acta*, *54*(12), 3525-3536. https://doi.org/10.1016/0016-7037(90)90302-2

Luais, B. (2012). Germanium chemistry and MC-ICPMS isotopic measurements of Fe–Ni, Zn alloys and silicate matrices: Insights into deep Earth processes. *Chemical Geology*, *334*, 295-311. https://doi.org/10.1016/j.chemgeo.2012.10.017

Luguet, A., Behrens, M., Pearson, D. G., König, S. & Herwartz, D. (2015). Significance of the whole rock Re–Os ages in cryptically and modally metasomatised cratonic peridotites: Constraints from HSE–Se–Te systematics. *Geochimica et Cosmochimica Acta*, *164*, 441-463. https://doi.org/10.1016/j.gca.2015.06.016

Makishima, A. & Nakamura, E. (2009). Determination of Ge, As, Se and Te in Silicate Samples Using Isotope Dilution-Internal Standardisation Octopole Reaction Cell ICP-QMS by Normal Sample Nebulisation. *Geostandards and Geoanalytical Research*, *33*(3), 369-384. https://doi.org/10.1111/j.1751-908X.2009.00014.x

Makishima, A., Tanaka, R. & Nakamura, E. (2009). Precise elemental and isotopic analyses in silicate samples employing ICP-MS: application of hydrofluoric acid solution and analytical techniques. *Analytical Sciences*, *25*(10), 1181-1187. https://doi.org/10.2116/analsci.25.1181

Marin, L., Lhomme, J. & Carignan, J. (2001). Determination of selenium concentration in sixty five reference materials for geochemical analysis by GFAAS after separation with thiol cotton. *Geostandards and Geoanalytical Research*, *25*(2-3), 317-324. https://doi.org/10.1111/j.1751-908X.2001.tb00608.x

Mcdonough, W. F. & Sun, S. S. (1995). The Composition of the Earth. *Chemical Geology*, *120*(3-4), 223-253. https://doi.org/10.1016/0009-2541(94)00140-4

Mcphail, D. C. (1995). Thermodynamic Properties of Aqueous Tellurium Species between 25 and 350 °C. *Geochimica et Cosmochimica Acta*, *59*(5), 851-866. https://doi.org/10.1016/00167-7037(94)00353-X

Meija, J., Coplen, T. B., Berglund, M., Brand, W. A., De Bievre, P., Groning, M., Holden, N. E., Irrgeher, J., Loss, R. D., Walczyk, T. & Prohaska, T. (2016). Isotopic compositions of the elements 2013 (IUPAC Technical Report). *Pure and Applied Chemistry*, *88*(3), 293-306. https://doi.org/10.1515/pac-2015-0503

Meisel, T. & Horan, M. F. (2016). Analytical Methods for the Highly Siderophile Elements. *Reviews in Mineralogy and Geochemistry*, *81*(1), 89-106. https://doi.org/10.2138/rmg.2016.81.02

Meisel, T., Reisberg, L., Moser, J., Carignan, J., Melcher, F. & Brügmann, G. (2003). Re–Os systematics of UB-N, a serpentinized peridotite reference material. *Chemical Geology*, *201*(1-2), 161-179. https://doi.org/10.1016/s0009-2541(03)00234-1

Mitchell, K., Mason, P. R. D., Van Cappellen, P., Johnson, T. M., Gill, B. C., Owens, J. D., Diaz, J., Ingall, E. D., Reichart, G. J. & Lyons, T. W. (2012). Selenium as paleo-oceanographic proxy: A first assessment. *Geochimica et Cosmochimica Acta*, *89*, 302-317. https://doi.org/10.1016/j.gca.2012.03.038

Mitchell, K., Mansoor, S. Z., Mason, P. R. D., Johnson, T. M. & Van Cappellen, P. (2016). Geological evolution of the marine selenium cycle: Insights from the bulk shale $\delta^{82/76}$Se record and isotope mass balance modeling. *Earth and Planetary Science Letters*, *441*, 178-187. https://doi.org/10.1016/j.epsl.2016.02.030

Moore, J. G. & Calk, L. (1971). Sulfide Spherules in Vesicles of Dredged Pillow Basalt. *American Mineralogist*, *56*(3-4), 476-488.

Morgan, J. W. (1986). Ultramafic xenoliths: Clues to Earth's late accretionary history. *Journal of*

Geophysical Research: Solid Earth, *91*(B12), 12375-12387. https://doi.org/10.1029/JB091iB12p12375

Pogge von Strandmann, P. A. E., Coath, C. D., Catling, D. C., Poulton, S. W. & Elliott, T. (2014). Analysis of mass dependent and mass independent selenium isotope variability in black shales. *Journal of Analytical Atomic Spectrometry*, *29*(9), 1648-1659. https://doi.org/10.1039/c4ja00124a

Pogge von Strandmann, P. A., Stüeken, E. E., Elliott, T., Poulton, S. W., Dehler, C. M., Canfield, D. E. & Catling, D. C. (2015). Selenium isotope evidence for progressive oxidation of the Neoproterozoic biosphere. *Nature Communications*, *6*(10157), 10157. https://doi.org/10.1038/ncomms10157

Rees, C. E. & Thode, H. G. (1966). Selenium Isotope Effects in the Reduction of Sodium Selenite and of Sodium Selenate. *Canadian Journal of Chemistry*, *44*(4), 419-427. https://doi.org/10.1139/v66-057

Rose-Weston, L., Brenan, J. M., Fei, Y. W., Secco, R. A. & Frost, D. J. (2009). Effect of pressure, temperature, and oxygen fugacity on the metal-silicate partitioning of Te, Se, and S: Implications for earth differentiation. *Geochimica et Cosmochimica Acta*, *73*(15), 4598-4615. https://doi.org/10.1016/j.gca.2009.04.028

Rouxel, O., Ludden, J., Carignan, J., Marin, L. & Fouquet, Y. (2002). Natural variations of Se isotopic composition determined by hydride generation multiple collector inductively coupled plasma mass spectrometry. *Geochimica et Cosmochimica Acta*, *66*(18), 3191-3199. https://doi.org/10.1016/S0016-7037(02)00918-3

Rouxel, O., Fouquet, Y. & Ludden, J. N. (2004). Subsurface processes at the Lucky Strike hydrothermal field, Mid-Atlantic Ridge: Evidence from sulfur, selenium, and iron isotopes. *Geochimica et Cosmochimica Acta*, *68*(10), 2295-2311. https://doi.org/10.1016/j.gca.2003.11.029

Rouxel, O., Galy, A. & Elderfield, H. (2006). Germanium isotopic variations in igneous rocks and marine sediments. *Geochimica et Cosmochimica Acta*, *70*(13), 3387-3400. https://doi.org/10.1016/j.gca.2006.04.025

Savard, D., Bedard, L. P. & Bames, S. J. (2009). Selenium Concentrations in Twenty-Six Geological Reference Materials: New Determinations and Proposed Values. *Geostandards and Geoanalytical Research*, *33*(2), 249-259. https://doi.org/10.1111/j.1751-908X.2009.00003.x

Schilling, K., Johnson, T. M. & Wilcke, W. (2011a). Isotope fractionation of selenium during fungal biomethylation by Alternaria alternata. *Environmental Science & Technology*, *45*(7), 2670-2676. https://doi.org/10.1021/es102926p

Schilling, K., Johnson, T. M. & Wilcke, W. (2011b). Selenium Partitioning and Stable Isotope Ratios in Urban Topsoils. *Soil Science Society of America Journal*, *75*(4), 1354. https://doi.org/10.2136/sssaj2010.0377

Schilling, K., Johnson, T. M. & Mason, P. R. D. (2014). A sequential extraction technique for mass-balanced stable selenium isotope analysis of soil samples. *Chemical Geology*, *381*, 125-130. doi:10.1016/j.chemgeo.2014.04.014

Schirmer, T., Koschinsky, A. & Bau, M. (2014). The ratio of tellurium and selenium in

geological material as a possible paleo-redox proxy. *Chemical Geology*, *376*, 44-51. doi:10.1016/j.chemgeo.2014.03.005

Schoenberg, R. & von Blanckenburg, F. (2005). An assessment of the accuracy of stable Fe isotope ratio measurements on samples with organic and inorganic matrices by high-resolution multicollector ICP-MS. *International Journal of Mass Spectrometry*, *242*(2-3), 257-272. https://doi.org/10.1016/j.ijms.2004.11.025

Schönbächler, M. & Fehr, M. A. (2014). Basics of Ion Exchange Chromatography for Selected Geological Applications. *Treatise on Geochemistry (Second Edition)*, 15, 123-146. https://doi.org/10.1016/b978-0-08-095975-7.01408-x

Stüeken, E. E., Foriel, J., Nelson, B. K., Buick, R. & Catling, D. C. (2013). Selenium isotope analysis of organic-rich shales: advances in sample preparation and isobaric interference correction. *Journal of Analytical Atomic Spectrometry*, *28*(11), 1734-1749. https://doi.org/10.1039/c3ja50186h

Stüeken, E. E., Buick, R. & Anbar, A. D. (2015a). Selenium isotopes support free O_2 in the latest Archean. *Geology*, *43*(3), 259-262. https://doi.org/10.1130/g36218.1

Stüeken, E. E., Buick, R., Bekker, A., Catling, D., Foriel, J., Guy, B. M., Kah, L. C., Machel, H. G., Montanez, I. P. & Poulton, S. W. (2015b). The evolution of the global selenium cycle: Secular trends in Se isotopes and abundances. *Geochimica et Cosmochimica Acta*, *162*, 109-125. https://doi.org/10.1016/j.gca.2015.04.033

Takei, H., Yokoyama, T., Makishima, A. & Nakamura, E. (2001). Formation and suppression of AlF_3 during HF digestion of rock samples in Teflon bomb for precise trace element analyses by ICP-MS and ID-TIMS. *Proceedings of the Japan Academy Series B: Physical and Biological Sciences*, *77*(1), 13-17.

Tokunaga, K., Yokoyama, Y. & Takahashi, Y. (2013). Estimation of Se(VI)/Se(IV) ratio in water by the ratio recorded in barite. *Geochemistry, Geophysics, Geosystems*, *14*(11), 4826-4834. https://doi.org/10.1002/ggge.20295

Vijan, P. N. & Leung, D. (1980). Reduction of Chemical Interference and Speciation Studies in the Hydride Generation Atomic-Absorption Method for Selenium. *Analytica Chimica Acta*, *120*(Nov), 141-146. https://doi.org/10.1016/S0003-2670(01)84356-7

Vollstaedt, H., Mezger, K. & Leya, I. (2016). The isotope composition of selenium in chondrites constrains the depletion mechanism of volatile elements in solar system materials. *Earth and Planetary Science Letters*, *450*, 372-380. https://doi.org/10.1016/j.epsl.2016.06.052

Wang, Z. & Becker, H. (2013). Ratios of S, Se and Te in the silicate Earth require a volatile-rich late veneer. *Nature*, *499*(7458), 328-331. https://doi.org/10.1038/nature12285

Wang, Z. C. & Becker, H. (2014). Abundances of Sulfur, Selenium, Tellurium, Rhenium and Platinum-Group Elements in Eighteen Reference Materials by Isotope Dilution Sector-Field ICP-MS and Negative TIMS. *Geostandards and Geoanalytical Research*, *38*(2), 189-209. https://doi.org/10.1111/j.1751-908X.2013.00258.x

Wang, Z. C. & Becker, H. (2015). Fractionation of highly siderophile and chalcogen elements during magma transport in the mantle: Constraints from pyroxenites of the Balmuccia peridotite massif. *Geochimica et Cosmochimica Acta*, *159*, 244-263.

https://doi.org/10.1016/j.gca.2015.03.036

Wang, Z. C. & Becker, H. (2017). Chalcophile elements in Martian meteorites indicate low sulfur content in the Martian interior and a volatile element-depleted late veneer. *Earth and Planetary Science Letters*, *463*, 56-68. https://doi.org/10.1016/j.epsl.2017.01.023

Wang, Z. C., Becker, H. & Gawronski, T. (2013). Partial re-equilibration of highly siderophile elements and the chalcogens in the mantle: A case study on the Baldissero and Balmuccia peridotite massifs (Ivrea Zone, Italian Alps). *Geochimica et Cosmochimica Acta*, *108*, 21-44. https://doi.org/10.1016/j.gca.2013.01.021

Wang, Z., Becker, H. & Wombacher, F. (2015). Mass Fractions of S, Cu, Se, Mo, Ag, Cd, In, Te, Ba, Sm, W, Tl and Bi in Geological Reference Materials and Selected Carbonaceous Chondrites Determined by Isotope Dilution ICP-MS. *Geostandards and Geoanalytical Research*, *39*(2), 185-208. https://doi.org/10.1111/j.1751-908X.2014.00312.x

Welz, B. & Melcher, M. (1984). Mechanisms of transition metal interferences in hydride generation atomic-absorption spectrometry Part 1. Influence of cobalt, copper, iron and nickel on selenium determination. *The Analyst*, *109*(5), 569. https://doi.org/10.1039/an9840900569

Wykes, J. L., O'Neill, H. C. & Mavrogenes, J. A. (2011). *XANES investigation of selenium speciation in silicate glasses.* Paper presented at Annual V. M. Goldschmidt Conference, Prague, Czech Republic

Wykes, J. L., O'Neill, H. S. C. & Mavrogenes, J. A. (2015). The Effect of FeO on the Sulfur Content at Sulfide Saturation (SCSS) and the Selenium Content at Selenide Saturation of Silicate Melts. *Journal of Petrology*, *56*(7), 1407-1424. https://doi.org/10.1093/petrology/egv041

Xu, G. P., Hannah, J. L., Bingen, B., Georgiev, S. & Stein, H. J. (2012). Digestion methods for trace element measurements in shales: Paleoredox proxies examined. *Chemical Geology*, *324*, 132-147. https://doi.org/10.1016/j.chemgeo.2012.01.029

Yi, W., Halliday, A. N., Lee, D. C. & Rehkamper, M. (1998). Precise determination of cadmium, indium and tellurium using multiple collector ICP-MS. *Geostandards and Geoanalytical Research*, *22*(2), 173-179. https://doi.org/10.1111/j.1751-908X.1998.tb00689.x

Yokoyama, T., Makishima, A. & Nakamura, E. (1999). Evaluation of the coprecipitation of incompatible trace elements with fluoride during silicate rock dissolution by acid digestion. *Chemical Geology*, *157*(3-4), 175-187. https://doi.org/10.1016/S0009-2541(98)00206-X

Yu, L. L., Fassett, J. D. & Guthrie, W. F. (2002). Detection limit of isotope dilution mass spectrometry. *Analytical Chemistry*, *74*(15), 3887-3891. https://doi.org/10.1021/ac011254l

Yu, M. Q., Liu, G. Q. & Jin, Q. (1983). Determination of Trace Arsenic, Antimony, Selenium and Tellurium in Various Oxidation-States in Water by Hydride Generation and Atomic-Absorption Spectrophotometry after Enrichment and Separation with Thiol Cotton. *Talanta*, *30*(4), 265-270. https://doi.org/10.1016/0039-9140(83)80060-5

Zhu, J.-M., Johnson, T. M., Clark, S. K. & Zhu, X.-K. (2008). High Precision Measurement of Selenium Isotopic Composition by Hydride Generation Multiple Collector Inductively Coupled Plasma Mass Spectrometry with a ^{74}Se-^{77}Se Double Spike. *Chinese Journal of Analytical Chemistry*, *36*(10), 1385-1390. https://doi.org/10.1016/s1872-2040(08)60075-4

Zhu, J. M., Johnson, T. M., Clark, S. K., Zhu, X. K. & Wang, X. L. (2014). Selenium redox

cycling during weathering of Se-rich shales: A selenium isotope study. *Geochimica et Cosmochimica Acta*, *126*, 228-249. https://doi.org/10.1016/j.gca.2013.11.004

Figure Captions

Figure 1. Elution profiles for Se (black line) and Te (blue line) from (a) standard solutions NIST SRM 3149 and 3156 and (b) BHVO-2 after the hotplate HF digestion using 7 mL of AG1-X8 and AG 50W-X8 anion and cation resins (100–200 mesh) following the newly established protocol in this study. The dashed lines represent the eluent we used. The relative fractions of Se and Te were determined at each 2.5 mL eluent (for 2 M HCl–5 M HF and 1 M HNO_3, 5 and 8 mL of fractions were collected, respectively) using ID method (supporting information Table S3). The Se–Te yields were determined twice on some collection cuts and the yield repeatabilities are <1% (r.s.d.). The Te elution with 1 M HNO_3 (Fehr et al., 2004; Wang et al., 2013) was additionally performed to check the complete desorption of Te from the resin during the column calibration.

Figure 2. BHVO-2 Se and Te concentrations analyzed from the HPA-S (inverse *aqua regia*) and different hotplate HF digestion procedures over the course of 18 months. These samples cover a wide range of sample sizes (~0.08–1.1 g). The sample size distributions are reported in supporting information Tables S1 and S6. Note that the reground sample powder shows the same Se and Te extraction efficiencies from the HPA-S digestion with the original/supplier powder, although they show quite distinct particle size distributions (supporting information Figure S1).

Figure 3. Effect of Fe on the hydride (H_2Te) formation efficiency in the hydride generator. The H_2Te formation yields of Fe-doped solutions are calculated by comparing signal intensities against those of pure NIST SRM 3156 standard solutions (0.5 ng mL^{-1}). It shows that H_2Te formation is highly sensitive to the amount of coexisting Fe. Based on this, the purified Te fraction from BHVO-2 (~15% difference between the column and overall recovery) is estimated to have residual Fe with Fe/Te mass ratio of ~1000–2000, which mainly accounts for the ~15% signal suppression.

Figure 4. The $\delta^{82/76}$Se value and Se concentrations of BHVO-2 obtained from the HPA-S (inverse *aqua regia*) and hotplate HF digestions. Horizontal error bars are internal precisions (2 s.e.) on $\delta^{82/76}$Se for a single analysis (40 cycles). The horizontal dashed lines and shaded fields represent average ID concentrations ± 1 s.d. obtained using each digestion method (Figure 1). The vertical dashed line and shaded field represent the bulk-rock average $\delta^{82/76}$Se value ± 2 s.d. that is obtained from HF digestions. Despite the systematically low Se extraction efficiency of the HPA-S

digestion (~76% relative to the HF digestion), the extracted fraction yields identical $\delta^{82/76}$Se value to that of the bulk rock.

Figure 5. The $\delta^{82/76}$Se values of reference materials analyzed using our newly established HF digestion and chromatographic purification protocols. Also shown for comparison are literature data for silicate rocks (Kurzawa et al., 2017; Rouxel et al., 2002, 2004), chondrites and troilites (Rouxel et al., 2002; Vollstaedt et al., 2016), as well as each chondrite group (Labidi et al., 2018). Literature data is converted to $\delta^{82/76}$Se relative to NIST SRM 3149 (Carignan & Wen, 2007). Horizontal error bars on our data represent 2 s.d. uncertainties estimated over at least 5 digestion batches and are well within our analytical precision of ~0.11‰. The grey shaded box represents the range for $\delta^{82/76}$Se values of analyzed basalts (0.23 ± 0.14‰), which is smaller but still falls in the previously constrained range (light-yellow shaded field) for the igneous silicate Earth (0.33 ± 0.32‰; Rouxel et al., 2002). Note that the range conservatively takes into account the 2 s.d. of the mean or, where larger, 2 s.d. analytical uncertainty.

Table 1.

Combined selenium isotope compositions and Se–Te concentrations of selected international reference materials analyzed from the same sample digests following the newly established hotplate HF digestion and chromatographic purification protocols in this study.

Samples		Se concentration[a] (ng g^{-1})	Se analyzed (ng)	$\delta^{82/76}$Se (‰)	2 s.e.[b] (‰)	Te concentration (ng g^{-1})
BHVO-2 (basalt)		171	14	0.21	0.06	14.3
		170	36	0.26	0.04	14.3
		167	12	0.18	0.11	14.3
		168	35	0.10	0.04	14.1
		168	37	0.14	0.04	14.2
		166	9	0.20	0.11	14.0
		166	20	0.16	0.06	14.1
		166	23	0.16	0.06	14.4
	Average	*169*		0.18		*14.2*
	Uncertainty[c]	*3*		0.10		*0.3*
König et al. (2012)		169 ± 3				11.9 ± 0.7
Wang et al. (2015)		170 ± 22				14.4 ± 0.3
BCR-2 (basalt)		76	15	0.28	0.06	2.50
		77	14	0.31	0.07	2.53
		78	13	0.36	0.07	2.46

		78	16	0.23	0.06	2.66
		77	17	0.25	0.06	2.52
	Average	*76*		0.29		2.54
	Uncertainty[c]	*1*		0.10		0.08
Makishima and Nakamura (2009)		82 ± 7				3.20 ± 0.04
Lissner et al. (2014)		78 ± 3				2.73 ± 0.06
Kurzawa et al. (2017)		71 ± 4		0.18 ± 0.03		
BE-N (basalt)		65	19	0.18	0.06	1.06
		66	20	0.16	0.05	1.04
		66	20	0.14	0.06	1.05
		65	20	0.20	0.05	1.03
		65	19	0.07	0.06	0.94
	Average	*66*		0.15		1.02
	Uncertainty[c]	*1*		0.10		0.05
Rouxel et al. (2002)		57		0.37 ± 0.32[d]		
Savard et al. (2009)		70 ± 9				
Lissner et al. (2014)		65 ± 1				0.82 ± 0.01
König et al. (2014)		67 ± 3				0.78 ± 0.10
BIR-1a (basalt)		14.9	18	0.25	0.08	5.86
		14.5	10	0.31	0.08	5.81
		15.4	18	0.28	0.08	5.85
		15.5	19	0.22	0.07	5.62
		14.5	12	0.36	0.08	5.98
	Average	15.0		0.28		5.82
	Uncertainty[c]	0.5		0.11		0.13
Yi et al. (1998)						5.70 ± 0.15
Forrest et al. (2009)		11–11.2				3.5–5.3
König et al. (2012)		14.2 ± 1.0				4.79 ± 0.17
W-2a (diabase)		107	21	−0.04	0.05	1.64
		108	27	−0.13	0.04	1.67
		108	41	−0.09	0.04	1.68
		107	30	−0.10	0.04	1.69
		108	18	−0.15	0.07	1.83
		106	24	0.00	0.05	1.75
	Average	*107*		−0.09		1.71
	Uncertainty[c]	*1*		0.11		0.07
Yi et al. (1998)						1.84 ± 0.05
Savard et al. (2009)		91 ± 13				
Forrest et al. (2009)		5.2				1.6

Italics refer to the average Se and Te concentrations and 1 s.d. calculated using the data in this table and all the additional Se and/or Te concentrations analyzed in this study from supporting information Table S6.

[a]Selenium concentrations in this table are obtained from the double-spike inversion.

[b]Internal precision of a sample run (over 40 cycles) is reported as 2 standard error (2 s.e.).

[c]All uncertainties are 2 s.d. and 1 s.d. for the average $\delta^{82/76}$Se and Se–Te concentrations, respectively.

[d]$\delta^{82/76}$Se data from Rouxel et al. (2002) is converted relative to NIST SRM 3149 following the approach of Carignan and Wen (2007).

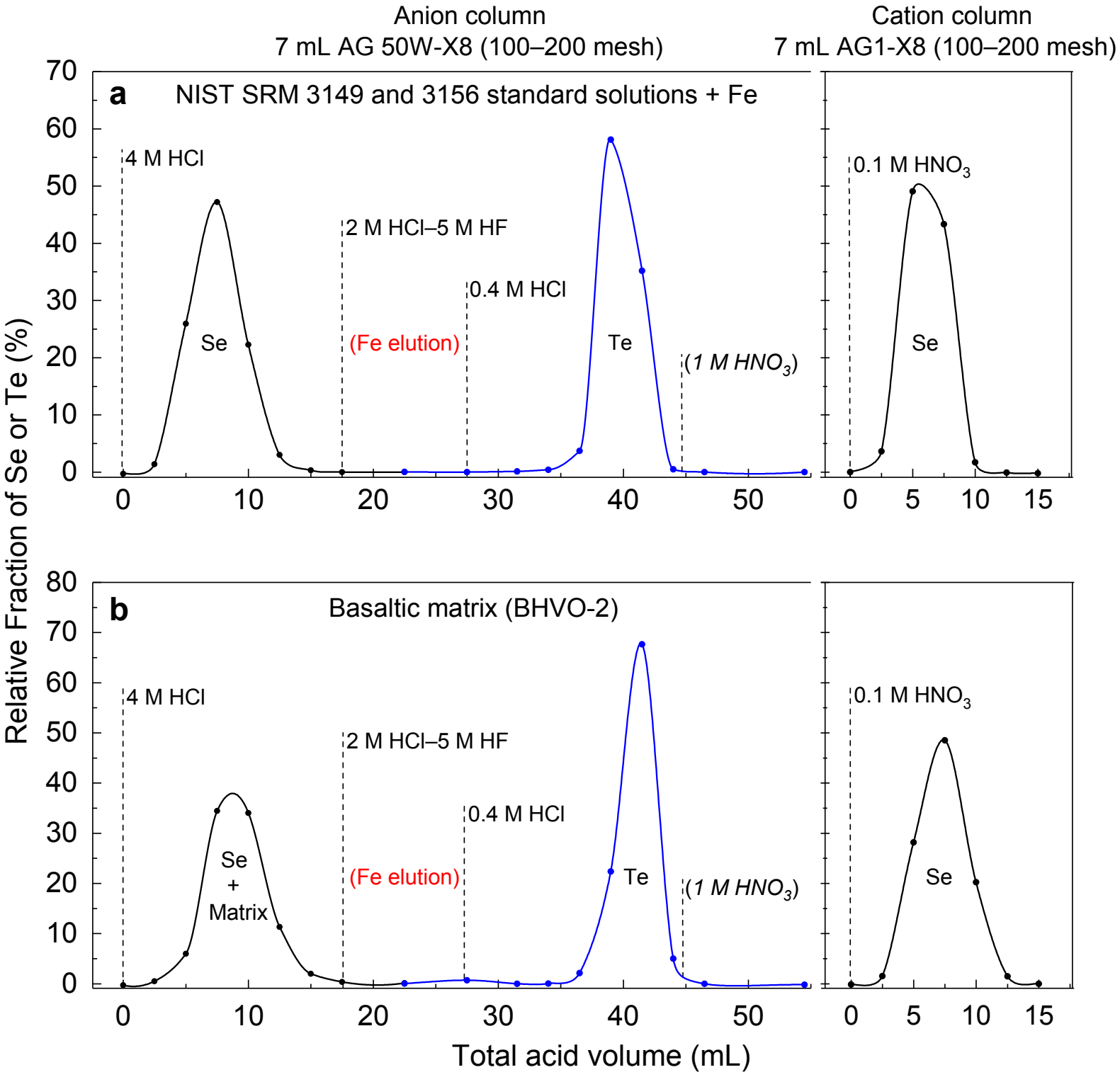
Anion column
7 mL AG 50W-X8 (100–200 mesh)
Cation column
7 mL AG1-X8 (100–200 mesh)
a
NIST SRM 3149 and 3156 standard solutions + Fe
4 M HCl
2 M HCl–5 M HF
0.4 M HCl
0.1 M HNO3
Se
(Fe elution)
Te
(1 M HNO3)
Se
b
Basaltic matrix (BHVO-2)
4 M HCl
2 M HCl–5 M HF
0.4 M HCl
0.1 M HNO3
Se + Matrix
(Fe elution)
Te
(1 M HNO3)
Se
Relative Fraction of Se or Te (%)
Total acid volume (mL)

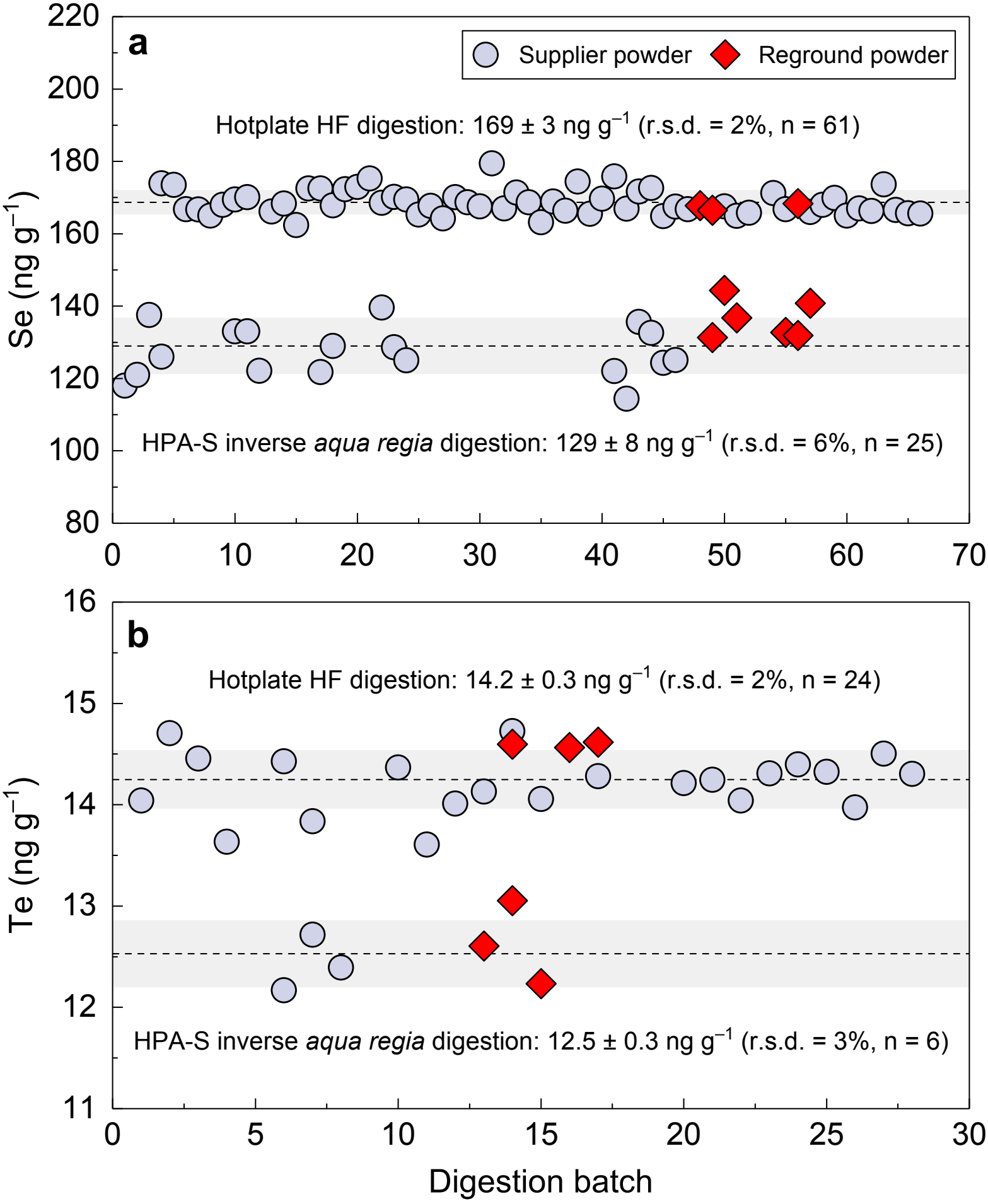
a
Supplier powder
Reground powder
Hotplate HF digestion: 169 ± 3 ng g−1 (r.s.d. = 2%, n = 61)
HPA-S inverse aqua regia digestion: 129 ± 8 ng g−1 (r.s.d. = 6%, n = 25)
Se (ng g−1)
220
200
180
160
140
120
100
80
0
10
20
30
40
50
60
70
b
Hotplate HF digestion: 14.2 ± 0.3 ng g−1 (r.s.d. = 2%, n = 24)
HPA-S inverse aqua regia digestion: 12.5 ± 0.3 ng g−1 (r.s.d. = 3%, n = 6)
Te (ng g−1)
16
15
14
13
12
11
0
5
10
15
20
25
30
Digestion batch

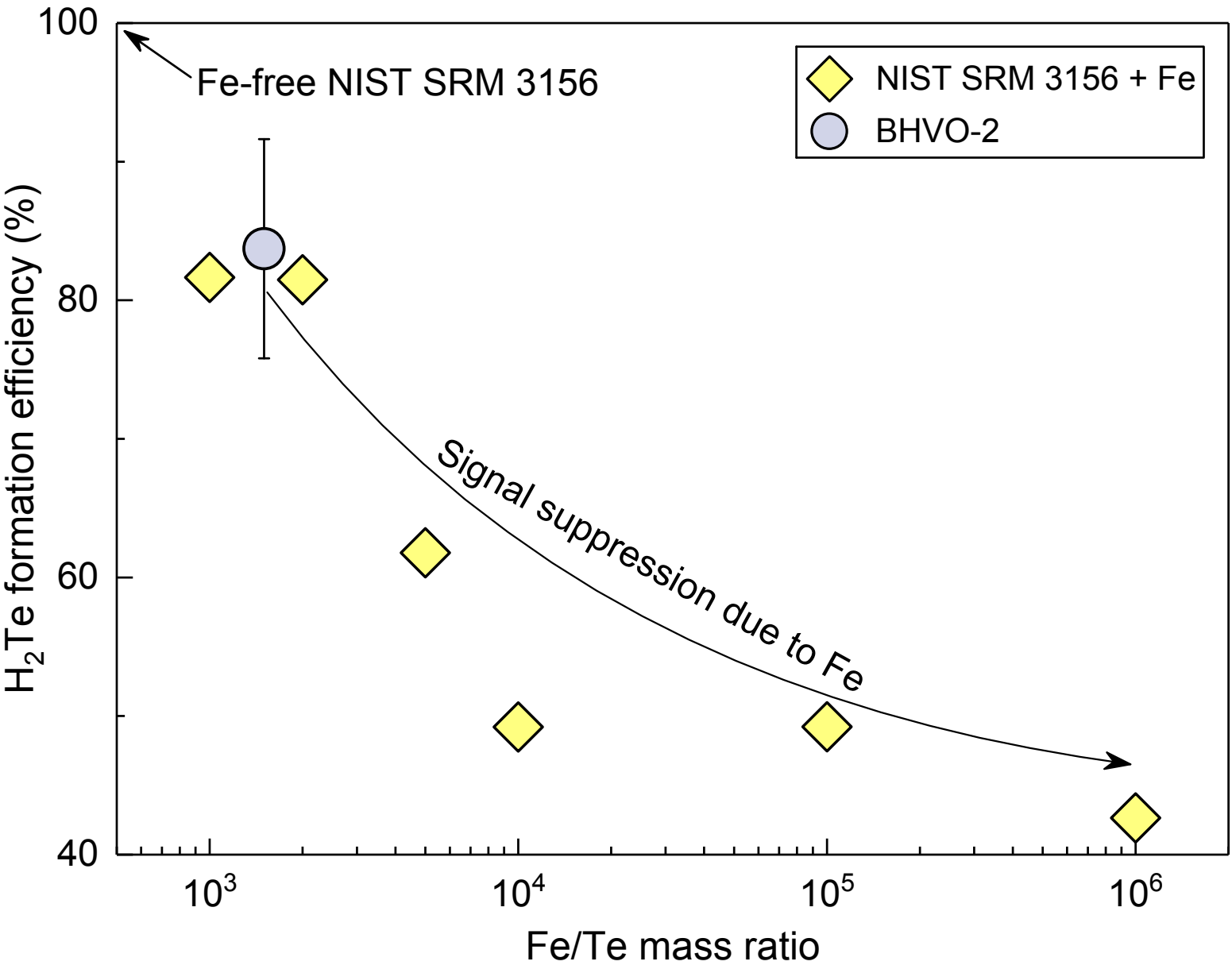
100
80
60
40
H_2Te formation efficiency (%)
Fe-free NIST SRM 3156
NIST SRM 3156 + Fe
BHVO-2
Signal suppression due to Fe
10^3
10^4
10^5
10^6
Fe/Te mass ratio

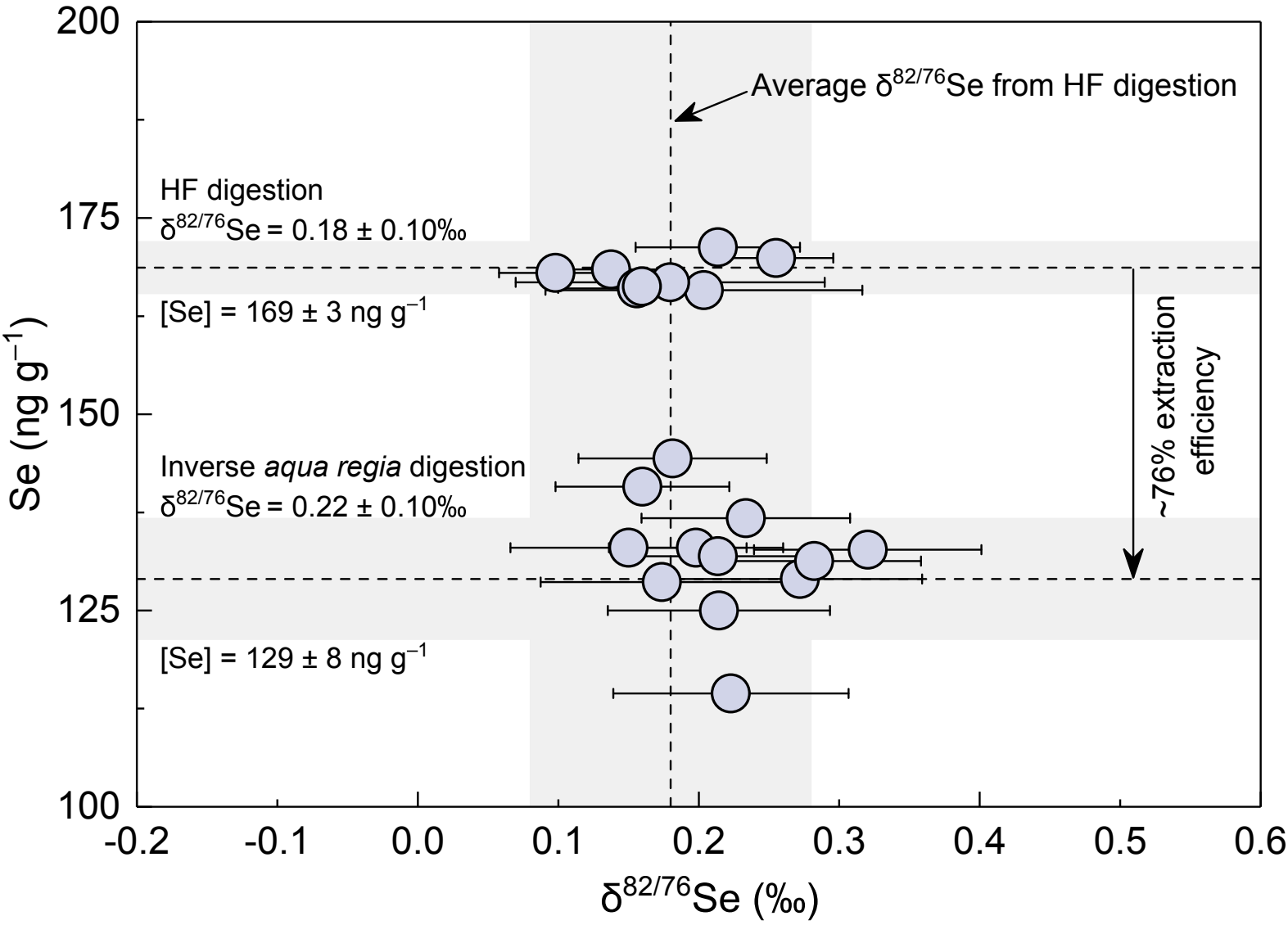
Average δ82/76Se from HF digestion
HF digestion
δ82/76Se = 0.18 ± 0.10‰
[Se] = 169 ± 3 ng g−1
Inverse aqua regia digestion
δ82/76Se = 0.22 ± 0.10‰
[Se] = 129 ± 8 ng g−1
~76% extraction efficiency
Se (ng g−1)
δ82/76Se (‰)
200
175
150
125
100
-0.2
-0.1
0.0
0.1
0.2
0.3
0.4
0.5
0.6

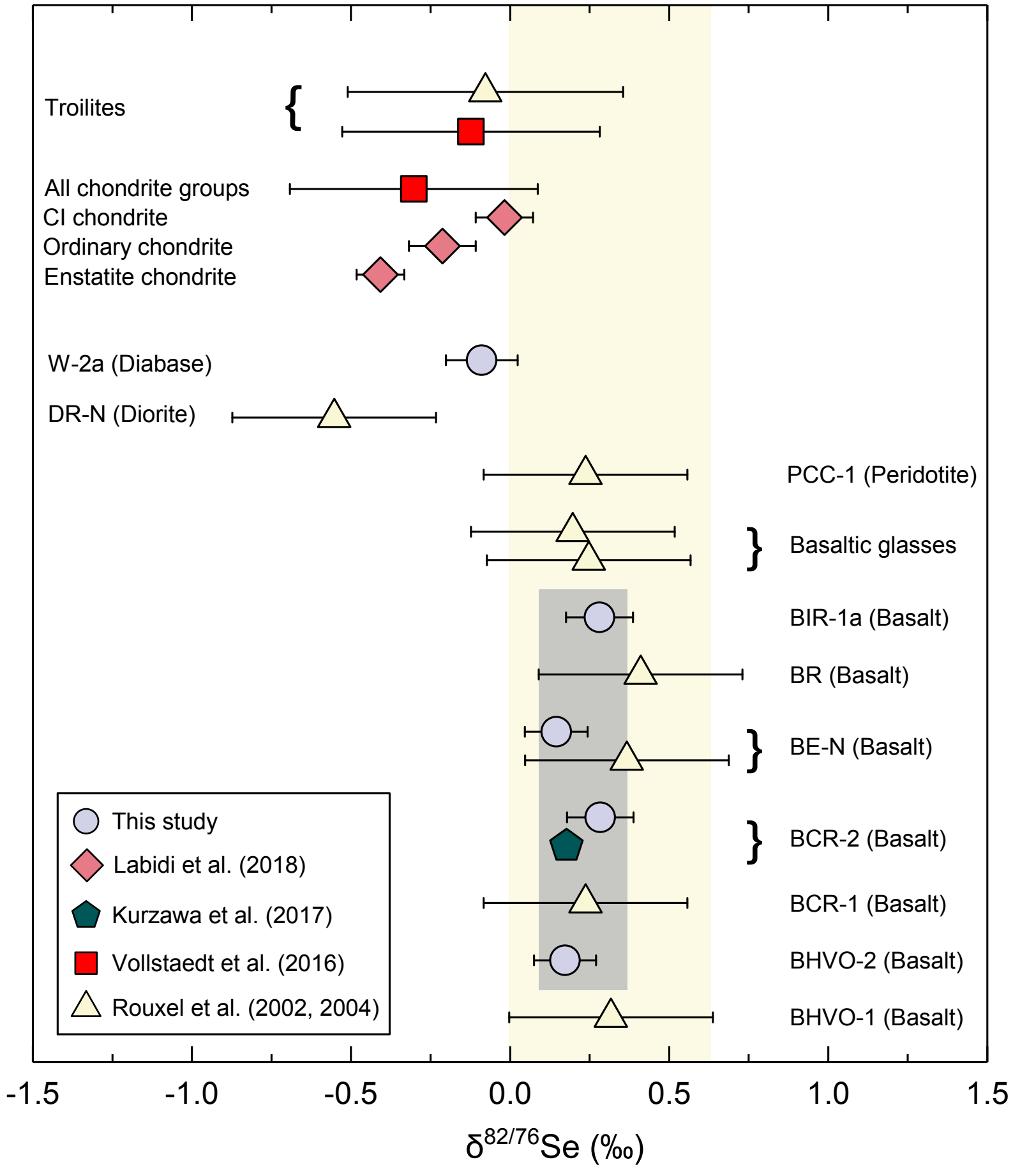
Troilites
All chondrite groups
CI chondrite
Ordinary chondrite
Enstatite chondrite
W-2a (Diabase)
DR-N (Diorite)
PCC-1 (Peridotite)
Basaltic glasses
BIR-1a (Basalt)
BR (Basalt)
BE-N (Basalt)
BCR-2 (Basalt)
BCR-1 (Basalt)
BHVO-2 (Basalt)
BHVO-1 (Basalt)
This study
Labidi et al. (2018)
Kurzawa et al. (2017)
Vollstaedt et al. (2016)
Rouxel et al. (2002, 2004)
-1.5
-1.0
-0.5
0.0
0.5
1.0
1.5
δ82/76Se (‰)

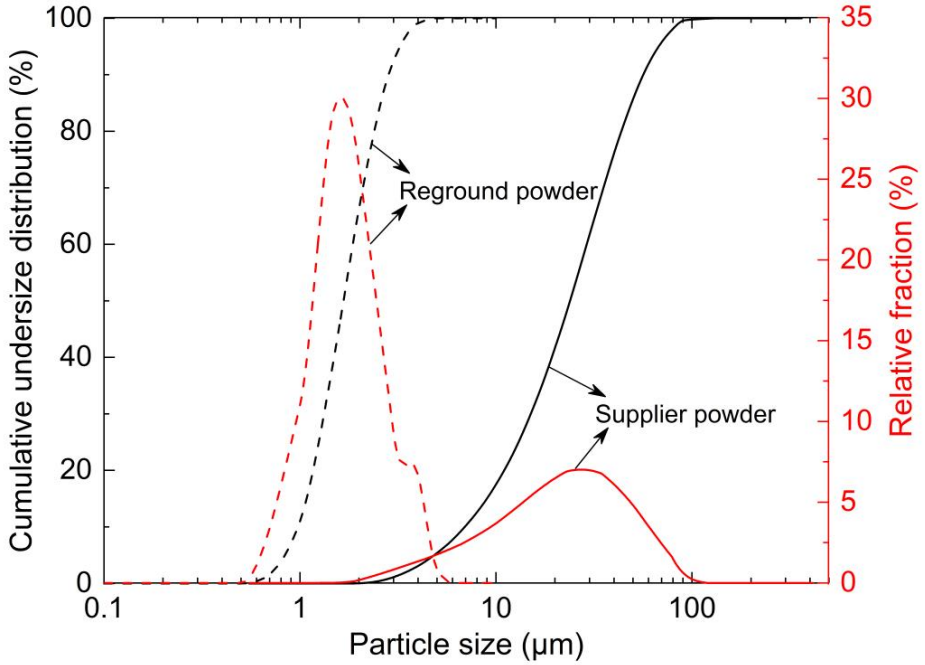

Figure S1. Comparison of particle size distribution of BHVO-2 between the supplier powder (provided by Stephen A. Wilson, USGS) and reground powder (analyzed using a laser particle sizer, Analysette 22 NanoTec, in the Application Laboratory of Fritsch, Germany). Note that all the reground powders have particles ≤5 μm. Although the particle size distribution is significantly different between these two rock powders, the same Se–Te extraction efficiency is observed from the HPA-S (inverse *aqua regia*) digestion.

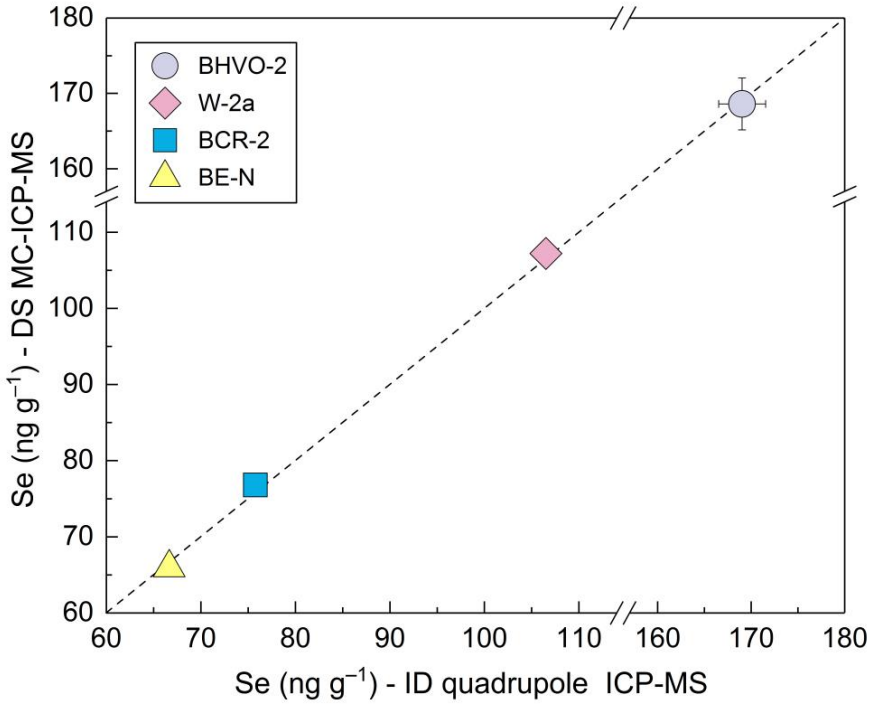

Figure S2. Comparison of Se concentrations (± 1 s.d.) determined by hydride generation DS MC-ICP-MS and ID quadrupole ICP-MS using aliquots from the same sample digest (Main text Table 1 and supporting information Table 6S). For all samples, the results are in excellent agreement (within ~3% variation) between both instruments. Note that the 1 s.d. uncertainties for BCR-2, BE-N and W-2a Se data are all smaller than the symbol size. The intermediate precision of our method is obtained from repeated analyses of BHVO-2 (75 analyses from 61 digestions) and is estimated to be ~2% (r.s.d.).

Table S1. Se–Te concentrations and/or Se isotope compositions analyzed for BHVO-2 supplier and reground powder with different sample sizes using HPA-S (inverse *aqua regia*) digestion conducted at 100 bar for 16 h. Also shown are Se concentrations analyzed for the undigested residue after the HPA-S procedure using HF digestion.

(Uploaded separately)

Table S2. Selenium and tellurium recoveries of BHVO-2 that are determined in this study from different chemical purification procedures following different sample digestion protocols.

Purification chemistry	Chromatography protocol used[a]	HPA-S inverse *aqua regia* digestion		Hotplate HF–HNO_3 digestion	
		Se recovery	Te recovery	Se recovery	Te recovery
TCF and TCP Chemistry[b]		-	-	<20% (n = 26)	-
Ion exchange chromatography					
Anion column chemistry[c]					
	A/B	55–81% (n = 15)	-	28–64% (n = 6)	54–58 % (n = 2)
	C	-	-	-	-
	new column chemistry	-	-	73–87% (n = 5)	85–93% (n = 5)
Cation column chemistry[d]					
	A/B	42–78% (n = 8)	-	-	-
	new column chemistry or C	-	-	92–100% (n = 5)	-
Overall procedural recovery[e]					
	A/B	39–57% (n = 15)	<10% (n = 6)	<20% (n = 6)	<20% (n = 15)
	C	-	-	-	~50% (n = 2)
	new column chemistry	-	-	70–83% (n = 16)	68–89% (n = 11)

[a]Chromatographic purification protocols for Se and/or Te: A = Kurzawa et al. (2017); B = Wang and Becker (2013); C = Wang et al. (2015). Each protocol was followed exactly as described in the original literature.
[b]See the text in detail for the protocol applied. In total, five TCF and 1 TCP batches (freshly-prepared before the purification) were used.
[c]Determined by ID when the sample is spiked after the anion column chemistry.
[d]Determined by signal comparison against NIST SRM 3149 solutions when (1) the sample is spiked after the anion column chemistry or (2) the sample is spiked prior to digestion and Se is measured separately from aliquots after anion- and cation-column chemistry.
[e]Determined by signal comparison of the final solution against NIST SRM 3149 and 3156 standard solutions for Se and Te, respectively. Note that it includes Se–Te recoveries from HCl evaporation at 85 °C, 2-stage column purification and hydride formation.

Table S3. Chromatographic separation of Se–Te using our newly established protocol from NIST SRM 3149 and 3156 mixture and BHVO-2 (after the HF digestion), and the relative recovery fractions[a] at each 2.5 mL eluent, which were used to obtain the elution profiles in Figure 1 in the main text.

Elution Step	Eluent	Volume[b] (mL)	Cumulative volume (mL)	Se (%)	Te (%)	Se (%)	Te (%)
Eichrom AG1-X8				NIST SRM 3149 and 3156 mixture		BHVO-2	
1	4M HCl	2.5	2.5	-		-	
2	4M HCl	2.5	5.0	25.9		6.0	
3	4M HCl	2.5	7.5	47.2		34.5	
4	4M HCl	2.5	10.0	22.3		34.0	
5	4M HCl	2.5	12.5	1.0		11.3	
6	4M HCl	2.5	15.0	0.1		1.6	
7	4M HCl	2.5	17.5	-		-	-
8	2M HCl–5M HF	5.0	22.5	<0.1	<0.1	-	<0.1
9	2M HCl–5M HF	5.0	27.5	<0.1	-		0.7
10	0.4 M HCl	4.0	31.5	-	0.2		-
11	0.4 M HCl	2.5	34.0		0.3		-
12	0.4 M HCl	2.5	36.5		3.7		-
13	0.4 M HCl	2.5	39.0		58.1		22.4
14	0.4 M HCl	2.5	41.5		35.2		67.6
15	0.4 M HCl	2.5	44.0		0.5		5.0
16	0.4 M HCl	2.5	46.5		-		1.0
17	1 M HNO_3[c]	8.0	54.5		-		-
Recovery				96.5	97.9	87.4	95.0
Eichrom AG 50W-X8				NIST SRM 3149		BHVO-2	
1	0.1 M HNO_3	2.5	2.5	3.61		0.2	
2	0.1 M HNO_3	2.5	5.0	49.1		28.2	
3	0.1 M HNO_3	2.5	7.5	43.3		48.5	
4	0.1 M HNO_3	2.5	10.0	1.3		20.2	
5	0.1 M HNO_3	2.5	12.5	<0.1		0.8	
6	0.1 M HNO_3	2.5	15.0	-		-	
Recovery				97.4		97.9	

[a]The relative recovery fractions were determined using ID method by spiking each individual eluent fraction after collection. The Se–Te yields were determined twice on some collection cuts and the yield repeatabilities are <1% (r.s.d.).

[b]The eluent fraction was collected at each 2.5 mL for 4 M HCl, 0.4 M HCl and 0.1 M HNO_3, 5 mL for 2M HCl–5M HF and 8 mL for 1M HNO_3.

[c]1 M HNO_3 was used to check if Te was completely eluted from the resin after the collection of 0.4 M HCl (see Fehr et al., 2004; Wang et al., 2015).

Table S4. The hydride (H_2Te) formation efficiencies[a] in the presence of different amount of Fe in 0.5 ng mL^{-1} NIST SRM 3156 standard solutions.

Fe/Te mass ratio	Hydride formation efficiency (%)
1000	82
2000	81
5000	62
10000	49
100000	49
1000000	43

[a]Efficiency of H_2Te formation in the hydride generation system (*hydrideICP*, *ESI*; 0.1 M $NaBH_4$–0.07 M NaOH and 2 M HCl) is calculated relative to Fe-free 0.5 ng mL^{-1} standard solutions.

Table S5. The $\delta^{82/76}Se$ value of the inter-laboratory standard MH 495 (15 and 30 ng mL^{-1} Se) measured together with the samples in this study.

(Uploaded separately)

Table S6. Compilation of Se and/or Te concentrations of BHVO-2, BCR-2, BE-N and W-2a that were measured using DS MC-ICP-MS and/or ID quadrupole ICP-MS from HF digestions using purification protocols existing in the literature and newly established in this study (see Figure 1 for details) over the course of 18 months.

(Uploaded separately)

Table S7. Se–Te concentrations of BHVO-2 sieved grain separates analyzed by ID quadrupole ICP-MS after the HF digestion and our newly established purification procedure.

BHVO-2 particle separates	Sieved weight fraction[a]		Se (ng g^{-1})	Te (ng g^{-1})
coarse particles (>25 μm)	49%			
			131	11.1
			135	10.3
			134	10.6
			132	
			136	
		Average concentration	134 ± 2[b]	10.6 ± 0.4[b]
		Se/Te	12.6 ± 0.5[b]	
fine particles (<25 μm)	51%			
			197	18.8
			203	19.3
			196	19.4
			193	18.2
			200	
			202	
			208	
		Average concentration	200 ± 5[b]	18.9 ± 0.5[b]
		Se/Te	10.6 ± 0.4[b]	
		Calculated bulk-rock concentration	167 ± 3[b]	14.8 ± 0.3[b]
		Measured bulk-rock concentration[c]	169 ± 3[b]	14.2 ± 0.3[b]
		Measured bulk-rock Se/Te	11.9 ± 0.7[b]	

[a]Normalized to 100%.
[b]All uncertainties are 1 s.d. for the average Se–Te concentrations and the calculated Se/Te ratios.
[c]It is taken from Table 1 in the main text.

Table S1

Se–Te concentrations and/or Se isotope compositions[a] analyzed for BHVO-2 supplier and reground powder with different sample sizes using HPA-S (inverse *aqua regia*) digestion conducted at 100 bar for 16 h. Also shown are Se concentrations analyzed for the undigested residue after the HPA-S procedure using HF digestion.

	Sample size (g)	Acid volume[b] (mL)	Digestion temperature (°C)		Se concentration (ng g^{-1})	$\delta^{82/76}$Se (‰)	2 s.e.[c] (‰)	Te concentration (ng g^{-1})	Dissolved powder fraction	Residue Se concentration (ng g^{-1})
Supplier powder										
	1.088	10.0	320		125					
	0.517	10.0	320		122					
	0.618	10.0	320		124					
	0.247	2.5	320		137					
	0.251	2.5	320		139					
	0.246	2.5	320		125					
	0.250	4.0	320		121					
	0.250	4.0	320		122					
	0.246	4.0	220		118					
	0.299	4.0	220		135					
	0.301	2.5	220		132					
	0.201	2.5	220		118					
	0.246	2.5	220		121					
	0.252	2.5	320		128	0.17	0.09			
	0.251	2.5	220		129	0.27	0.09			
	0.250	2.5	220		133	0.19	0.06			
	0.250	2.5	220		133	0.15	0.08			
	0.257	2.5	220		124	0.21	0.08			
	0.307	2.5	220		114	0.22	0.08		15%	41
	0.763	10.0	280					12.2	9%	
	0.745	7.5	280					12.2	10%	
	0.753	7.5	280					12.7	10%	
				Average	127	0.21		12.4		
				Uncertainty[d]	7	0.08		0.3		
Reground powder										
	0.302	4.0	220		133	0.32	0.08		17%	35
	0.302	2.5	220		132	0.21	0.07		13%	37
	0.302	2.5	220		131	0.28	0.08		16%	35
	0.307	2.5	220		144	0.18	0.07		15%	40
	0.302	2.5	220		137	0.23	0.07		10%	33
	0.305	2.5	220		141	0.16	0.06		14%	40
	0.756	10.0	280					12.4	9%	
	0.764	7.5	280					13.1	9%	
	0.759	7.5	280					12.6	10%	
				Average	136	0.23		12.7		
				Uncertainty[d]	5	0.12		0.3		
				Total average	129	0.22		12.5	12%	37
				Uncertainty[d]	8	0.10		0.3	3%	3
				n	25	12		6	13	7

[a]In contrast to data listed in Table 1, Te concentration and Se isotope (hence Se isotope concentration) were not determined from the same sample digest from the HPA-S (inverse *aqua regia*) digestion as the purpose of this experiment is to assess the Se–Te extraction efficiencies.

[b]Acid mixture of 14.5 M HNO_3 and 10.5 M HCl (molar ratio 3:1).

[c]Internal precision of a sample run during Se isotope analysis (over 40 cycles) is reported as 2 standard error (2 s.e.).
[d]Uncertainties are 2 s.d. for $\delta^{82/76}$Se and 1 s.d. for all other data.

Table S5

The $\delta^{82/76}$Se value of the inter-laboratory standard MH 495 (15 and 30 ng mL^{-1} Se) measured together with the samples in this study.

	15 ng mL^{-1} solution		30 ng mL^{-1} solution	
	$\delta^{82/76}$Se (‰)	2 s.e.[a] (‰)	$\delta^{82/76}$Se (‰)	2 s.e.[a] (‰)
	-3.14	0.07	-3.24	0.04
	-3.27	0.06	-3.30	0.05
	-3.26	0.07	-3.28	0.05
	-3.19	0.06	-3.26	0.04
	-3.20	0.06	-3.22	0.04
	-3.15	0.05	-3.23	0.03
	-3.26	0.06	-3.25	0.04
	-3.21	0.05	-3.26	0.05
	-3.25	0.06	-3.27	0.03
	-3.21	0.07	-3.27	0.05
	-3.18	0.05	-3.20	0.03
	-3.24	0.06	-3.26	0.04
	-3.27	0.06	-3.25	0.03
	-3.29	0.07	-3.23	0.05
	-3.23	0.06	-3.27	0.04
	-3.12	0.06	-3.28	0.04
	-3.17	0.06	-3.26	0.03
	-3.18	0.06	-3.26	0.05
	-3.32	0.08	-3.33	0.05
	-3.26	0.07	-3.24	0.05
	-3.26	0.05	-3.22	0.04
	-3.25	0.05	-3.27	0.04
	-3.34	0.07	-3.26	0.04
	-3.28	0.06	-3.24	0.05
	-3.22	0.06	-3.29	0.05
	-3.19	0.07	-3.27	0.04
	-3.25	0.07	-3.25	0.04
	-3.30	0.06	-3.30	0.04
	-3.30	0.06	-3.31	0.05
	-3.23	0.07	-3.28	0.05
	-3.20	0.07	-3.24	0.05
	-3.20	0.08	-3.23	0.05
	-3.21	0.07		
	-3.19	0.06		
	-3.24	0.07		
	-3.25	0.07		
	-3.27	0.07		
	-3.26	0.07		
	-3.27	0.08		
	-3.17	0.07		
	-3.28	0.06		
	-3.27	0.05		
	-3.24	0.06		
	-3.29	0.07		
	-3.27	0.07		
	-3.21	0.06		
Average	-3.24		-3.26	
2 s.d.	0.10		0.06	
	n = 46		n = 32	

[a]Internal precision of a sample run during Se isotope analysis (over 40 cycles) is reported as 2 standard error (2 s.e.).

Table S6

Compilation[a] of Se and/or Te concentrations of BHVO-2, BCR-2, BE-N and W-2a that were measured using DS MC-ICP-MS and/or ID quadrupole ICP-MS (iQAP-Q) from HF digestions using purification protocols existing in the literature and newly established in this study (see Figure 1 for details) over the course of 18 months.

Sample	Digestion batch	Sample size (g)	Purification protocol used[b,c]	Se concentration(ng g^{-1})	ICP-MS used for Se analysis	Te concentration(ng g^{-1})
BHVO-2	1	0.243	A (2-stage)	174	Neptune	
BHVO-2	2	0.246	A (2-stage)	173	Neptune	
BHVO-2	3	0.084	A (1st stage)	167	iQAP-Q	
BHVO-2	4	0.084	A (1st stage)	167	iQAP-Q	
BHVO-2	5	0.255	A (1st stage)	165	Neptune	
BHVO-2	6	0.253	A (1st stage)	168	Neptune	
BHVO-2	7	0.252	A (1st stage)	169	Neptune	
	7		A (1st stage)	170	iQAP-Q	
	7		A (2-stage)	170	Neptune	
BHVO-2	8	0.380	A (1st stage)	170	Neptune	
	8		A (1st stage)	170	iQAP-Q	
	8		A (2-stage)	170	Neptune	
	8		A (2-stage)	170	Neptune	
BHVO-2	9	0.251	B (2-stage)	168	Neptune	
BHVO-2	10	0.252	A (2-stage)	166	Neptune	
BHVO-2	11	0.251	A (1st stage)	168	Neptune	
BHVO-2	12	0.253	A (2-stage)	162	Neptune	
BHVO-2	13	0.258	A (1st stage)	172	Neptune	
BHVO-2	14	0.258	A (1st stage)	172	iQAP-Q	
BHVO-2	15	0.206	A (1st stage)	168	iQAP-Q	
	15		A (1st stage)	169	iQAP-Q	
BHVO-2	16	0.218	A (1st stage)	172	iQAP-Q	
BHVO-2	17	0.262	A (1st stage)	173	iQAP-Q	
BHVO-2	18	0.209	A (1st stage)	175	iQAP-Q	
BHVO-2	19	0.251	A (1st stage)	169	iQAP-Q	
BHVO-2	20	0.275	B (2-stage)	170	iQAP-Q	14.5
	20		A (1st stage)	170	iQAP-Q	
BHVO-2	21	0.269	A (1st stage)	169	iQAP-Q	
BHVO-2	22	0.300	A (1st stage)	165	Neptune	
BHVO-2	23	0.262	C			13.6
BHVO-2	24	0.267	C			13.8
BHVO-2	25	0.250	B (1st stage)			14.7
BHVO-2-reground	26	0.250	B (2-stage)	168	iQAP-Q	14.6
	26		A (2-stage)	168	iQAP-Q	
	26		A (2-stage)	171	Neptune	
BHVO-2	27	0.205	TCF	164	Neptune	
BHVO-2	28	0.231	B (1st stage)			14.4
BHVO-2	29	0.229	B (2-stage)	170	iQAP-Q	14.4
	26		A (1st stage)	171	iQAP-Q	
	26		A (1st stage)	170	iQAP-Q	

BHVO-2	30	0.304	A (1st stage)	169	iQAP-Q	
BHVO-2	31	0.247	B (1st stage)	168	iQAP-Q	14.0
BHVO-2	32	0.104	A (1st stage)	167	iQAP-Q	
BHVO-2	33	0.110	A (1st stage)	171	iQAP-Q	
BHVO-2	34	0.255	B (1st stage)			13.6
BHVO-2	35	1.114	A (2-stage)	169	Neptune	
BHVO-2	36	1.012	TCF	174	Neptune	
BHVO-2	37	1.105	TCF	169	Neptune	
BHVO-2	38	1.035	TCF	166	Neptune	
BHVO-2	39	1.024	TCF	170	Neptune	
BHVO-2	40	0.521	TCF	166	Neptune	
BHVO-2	41	0.510	TCP	163	Neptune	
BHVO-2	42	1.008	TCP	176	Neptune	
BHVO-2	43	1.011	TCP	172	Neptune	
BHVO-2	44	0.501	new column chemistry	167	Neptune	
BHVO-2	45	0.500	new column chemistry	167	Neptune	
BHVO-2	46	0.238	new column chemistry	165	Neptune	
BHVO-2	47	0.101	new column chemistry	173	Neptune	
BHVO-2	48	0.102	new column chemistry	168	Neptune	
BHVO-2-reground	49	0.426	new column chemistry	165	iQAP-Q	14.6
BHVO-2-reground	50	0.405	new column chemistry	167	iQAP-Q	14.6
BHVO-2	51	0.309	new column chemistry	165	Neptune	
BHVO-2	52	0.302	new column chemistry	179	Neptune	
BHVO-2	53	0.204	new column chemistry	168	Neptune	
BHVO-2	54	0.245	new column chemistry	167	Neptune	14.3
	54		new column chemistry	166	iQAP-Q	
BHVO-2	55	0.245	new column chemistry	167	Neptune	14.3
	55		new column chemistry	166	iQAP-Q	
BHVO-2	56	0.248	new column chemistry	166	Neptune	14.0
	56		new column chemistry	166	iQAP-Q	
BHVO-2	57	0.224	new column chemistry	166	Neptune	14.5
BHVO-2	58	0.230	new column chemistry	174	Neptune	14.3
			Average	**169**		**14.3**
			1 s.d.	3		0.3
			n[d]	53		16
BCR-2	1	1.216	A (1st stage)	75	iQAP-Q	
	1		A (1st stage)	75	iQAP-Q	
	1		A (1st stage)	76	iQAP-Q	
	1		A (1st stage)	76	iQAP-Q	
	1		A (1st stage)	76	iQAP-Q	
	1		A (1st stage)	76	iQAP-Q	
	1		A (2-stage)	75	iQAP-Q	
	1		A (2-stage)	75	iQAP-Q	
	1		A (2-stage)	75	iQAP-Q	
	1		A (2-stage)	74	iQAP-Q	
BCR-2	2	0.853	A (1st stage)	75	iQAP-Q	

BCR-2	3	1.019	TCF	75	Neptune
BCR-2	4	1.100	TCF	76	Neptune
BCR-2	5	1.036	TCP	78	Neptune
BCR-2	6	1.039	TCP	76	Neptune
BCR-2	7	0.748	new column chemistry	78	Neptune
BCR-2	8	0.735	new column chemistry	78	Neptune
BCR-2	9	0.347	new column chemistry	76	Neptune
BCR-2	10	0.356	new column chemistry	76	Neptune
BCR-2	11	0.351	new column chemistry	77	Neptune
	11		new column chemistry	77	iQAP-Q
BCR-2	12	0.328	new column chemistry	78	iQAP-Q
BCR-2	13	0.329	new column chemistry	77	iQAP-Q
			Average	**76**	
			1 s.d.	1	
			n[d]	13	
BE-N	1	0.204	new column chemistry	67	iQAP-Q
BE-N	2	0.598	new column chemistry	66	Neptune
BE-N	3	0.602	new column chemistry	67	Neptune
BE-N	4	0.627	new column chemistry	66	Neptune
BE-N	5	0.399	new column chemistry	65	Neptune
BE-N	6	0.399	new column chemistry	65	Neptune
BE-N	7	0.402	new column chemistry	63	Neptune
BE-N	8	0.401	new column chemistry	65	Neptune
BE-N	9	0.865	new column chemistry	67	Neptune
BE-N	10	0.851	new column chemistry	68	Neptune
BE-N	11	0.861	new column chemistry	66	Neptune
BE-N	12	0.429	new column chemistry	66	Neptune
BE-N	13	0.463	new column chemistry	67	Neptune
BE-N	14	0.398	new column chemistry	66	Neptune
BE-N	15	0.386	new column chemistry	67	Neptune
BE-N	16	0.335	new column chemistry	67	Neptune
BE-N	17	0.400	new column chemistry	64	Neptune
BE-N	18	0.517	new column chemistry	66	Neptune
	18		new column chemistry	66	iQAP-Q
			Average	**66**	
			1 s.d.	1	
			n[d]	18	
W-2a	1	0.309	new column chemistry	106	iQAP-Q
W-2a	2	0.275	new column chemistry	107	iQAP-Q
			Average	**107**	
			1 s.d.	1	
			n[d]	2	

[a]Note that, in this table, the samples processed after the new column chemistry were only analyzed for additional Se concentrations (Se isotopes and/or Te concentration analyses were not performed) for a more reliable evaluation of the accuracy and precision of our routine Se concentration analysis. Se–Te concentrations determined together with the Se isotope composition from the same sample digests are reported in Table 1 and are not further included here.

[b]A = Kurzawa et al. (2017); B =Wang and Becker (2013); C = Wang et al. (2015). Each protocol was followed exactly as described

in the original literature.

[c]2-stage = anion + cation exchange column; 1st stage = anion exchange column only.

[d]Number of digestion repeats.